

Response to Referee #1

We are grateful to the reviewer for their time and energy in providing helpful comments and guidance that have improved the manuscript. In this document, we describe how we have addressed the reviewer's comments. Referee comments are shown in black italics and author responses are shown in blue regular text.

This paper represents valuable evaluations of the changes in major land carbon fluxes and plant volatile emissions, and interesting analysis of the causes behind those trends using the latest YIBs model. The topic is important and the work is very systematic. The reviewer recommends acceptance with minor revisions based upon the suggestions mentioned below.

1. For the section 2.1 in Page 21453, the MTE GPP product was not derived from any biosphere model. Please refer to (Jung et al., 2009) and put correct description.

→ We have corrected it as “GPP benchmark products of 1982-2011 are upscaled from the FLUXNET eddy covariance measurements using an ensemble of regression trees (Jung et al., 2009)”.

2. Please let the readers know whether those regional trends in Table 2 and 3 are significant.

→ We have added “asterisks” to indicate the significant ($p < 0.05$) changes for trends.

3. In the Results part, the authors compared YIBs simulations with a lot of previous work, such as Sitch et al. (2015), Pan et al. (2011), Stavrou et al. (2014), Naik et al. (2004), and Jeong et al., 2011. Please subtract them and merge them into the Discussion.

→ We have moved most comparisons, e.g. Sitch et al. (2015), Stavrou et al. (2014), and Naik et al. (2004) to a new discussion section “4.2 Comparisons with other modeling studies”. We retained comparisons with Pan et al. (2011) and Jeong et al. (2011) because these are based on observations and useful to validate our simulation results.

Response to Referee #2

We are grateful to the reviewer for their time and energy in providing helpful comments and guidance that have improved the manuscript. In this document, we describe how we have addressed the reviewer's comments. Referee comments are shown in black italics and author responses are shown in blue regular text.

The paper addresses the trends in carbon and BVOC fluxes in the YIBs model. Although the research methods are sound and the topic one of general interest to the community, at the end of the paper, it was unclear what the guiding scientific question was. If the goal of the paper was to provide an improved accounting of carbon fluxes beyond what other models could provide, the paper did not put the YIBs results in the context of other models or previous works. This is a major deficit.

If the main science question relates to what does YIBs predict for carbon fluxes, the authors don't tell the reader why s/he should care about this specific model. The paper is a length description of simulations that test the trends in carbon fluxes using two different reanalysis driver data sets, but also conduct experiments with climate change alone, CO₂ fertilization, and land use change, before isolating LAI as a driver of carbon fluxes. Separating these drivers is important, but the paper as a result is very unfocused. Many of the figures needed to support their results are supplementary, and this diminishes the main text. The authors should revise this paper to make it clear what the science questions are and structure the results in a more organized fashion.

→ The main purpose of this study is to quantify the drivers of 30-year trends in land carbon flux and BVOC emissions. We agree that some of the analyses and discussions are not well organized, leading to distractions from this major goal. In the revised paper, we have made changes in the following four aspects:

(a) We clearly narrated that: “The major goals of this study are to identify: (1) the dominant drivers of the 30-year trends in carbon fluxes and BVOC emissions from elevated CO₂, changes in meteorology (temperature, radiation, and soil moisture), and human land use change; (2) the feedback of biosphere, including changes in phenology and leaf area index (LAI), to the trends of land carbon uptakes and BVOC emissions; and (3) the discrepancies in BVOC trends due to application of different isoprene emission schemes.”

(b) We changed subtitles of section 3 as follows: “3.1 Drivers of trends in LAI”, “3.2 Drivers of trends in land carbon fluxes”, “3.3 Drivers of trends in BVOC emissions”, “3.4 Feedback of biospheric changes to the trends”. These changes emphasize that we are exploring the drivers of trend, instead of the trend itself.

(c) We moved all inter-model comparisons to a new discussion section 4.2. In this way, we avoid misleading readers that we are performing inter-model comparisons or model evaluation studies.

(d) We removed all simulation results using MERRA. The changes include the revision of Figure 4 and removal of Figure S1, S3, S4, and Table S1. We also deleted long paragraphs in section 3.2 and original section 4.3 (now 4.4). In the original manuscript, we compared model results driven with two reanalyses, WFDEI and MERRA. We meant to assess the model uncertainties due to meteorological forcings. However, such comparison may mislead readers that we are trying to improve the trend prediction, instead of examining the drivers behind the trend.

The paper states that the YIBs model is "well-validated", but the authors owe it to their readers to describe the methodology and results of their previous validation exercises, which is merely cited here. Given that the YIBs model is not perfect, the authors should identify both the areas where YIBs had largest disagreement with their validation data and where it was in best agreement.

→ We presented more descriptions about the YIBs model in the revised manuscript.

(a) In the introduction section, we added: “In this study, we use the Yale Interactive Terrestrial Biosphere Model (YIBs, Yue and Unger, 2015) driven with long-term reanalysis meteorology to study the global trends of land carbon fluxes and BVOC emissions over the past three decades. The YIBs model is a process-based vegetation model including complete land carbon cycle (photosynthesis, plant/soil respiration, carbon allocation, and tree growth), plant phenology (Yue et al., 2015), and two independent schemes of BVOC emissions (Zheng et al., 2015). Simulated carbon fluxes has been fully validated with carbon fluxes from 145 flux tower sites and multiple satellite products (Yue and Unger, 2015).”

(b) In the last paragraph of method section 2.2, we added: “At the site level, YIBs simulates reasonable seasonality (correlation coefficient $R > 0.8$) of GPP at 121 out of 145 flux-tower sites with biases in magnitude ranging from -19 to 7 % depending on PFTs. On the global scale, the offline model simulates an annual GPP of 125 ± 3 Pg C and net ecosystem exchange (NEE) of -2.5 ± 0.7 Pg C for 1982-2011, with seasonality and spatial distribution consistent with both satellite observations and benchmark synthesis products (Yue and Unger, 2015). However, the model does not include a fully coupled carbon-nitrogen cycle, which may overestimate CO₂ fertilization effects. In addition, phenology of evergreen trees is set to constant value of 1, leading to underestimation of phenological feedbacks to flux trends.”

On p21471, the authors state that "Our results show the large climate-driven uncertainties in the estimate of long-term trends... indicating the necessity of forcing inter-comparisons in addition to model inter-comparisons". The authors have not provided much analysis on whether there is some switch in the YIBs model that has a non-linear sensitivity to a small change in reanalysis observations used.

→ This sentence has been deleted as we have removed the comparisons of modeling results with two meteorological reanalysis datasets, which is not closely related to the main focus of the study.

The authors describe the GPP product as an observation, but it is not an observation. Perhaps it is more accurate to call it a "benchmark" than an "observation".

→ We have changed the GPP “observation” to “benchmark product”.

The multi-panel figures with maps have too much white space and tentially the maps are too small.

→ The reason why there is white space on these figures is that we plot only the statistically significant changes ($p < 0.05$). We do not wish to distract readers' attention by showing changes that are not statistically robust. We have modified the display structure (from 3 columns by 2 rows to 2 columns by 3 rows) of Figures 1, 2, and 6 to enlarge maps.

Reference

- Jeong, S. J., Ho, C. H., Gim, H. J., and Brown, M. E.: Phenology shifts at start vs. end of growing season in temperate vegetation over the Northern Hemisphere for the period 1982-2008, *Global Change Biol*, 17, 2385-2399, doi:10.1111/J.1365-2486.2011.02397.X, 2011.
- Naik, V., Delire, C., and Wuebbles, D. J.: Sensitivity of global biogenic isoprenoid emissions to climate variability and atmospheric CO₂, *J. Geophys. Res.*, 109, D06301, doi:10.1029/2003jd004236, 2004.
- Pan, Y. D., Birdsey, R. A., Fang, J. Y., Houghton, R., Kauppi, P. E., Kurz, W. A., Phillips, O. L., Shvidenko, A., Lewis, S. L., Canadell, J. G., Ciais, P., Jackson, R. B., Pacala, S. W., McGuire, A. D., Piao, S. L., Rautiainen, A., Sitch, S., and Hayes, D.: A Large and Persistent Carbon Sink in the World's Forests, *Science*, 333, 988-993, doi:10.1126/Science.1201609, 2011.
- Sitch, S., Friedlingstein, P., Gruber, N., Jones, S. D., Murray-Tortarolo, G., Ahlström, A., Doney, S. C., Graven, H., Heinze, C., Huntingford, C., Levis, S., Levy, P. E., Lomas, M., Poulter, B., Viovy, N., Zaehle, S., Zeng, N., Arneeth, A., Bonan, G., Bopp, L., Canadell, J. G., Chevallier, F., Ciais, P., Ellis, R., Gloor, M., Peylin, P., Piao, S. L., Quéré, C. L., Smith, B., Zhu, Z., and Myneni, R.: Recent trends and drivers of regional sources and sinks of carbon dioxide, *Biogeosciences*, 12, 653-679, 2015.
- Stavrakou, T., Muller, J. F., Bauwens, M., De Smedt, I., Van Roozendaal, M., Guenther, A., Wild, M., and Xia, X.: Isoprene emissions over Asia 1979-2012: impact of climate and land-use changes, *Atmos Chem Phys*, 14, 4587-4605, doi:10.5194/Acp-14-4587-2014, 2014.
- Yue, X., and Unger, N.: The Yale Interactive terrestrial Biosphere model: description, evaluation and implementation into NASA GISS ModelE2, *Geosci. Model Dev.*, 8, 2399-2417, doi:10.5194/gmd-8-2399-2015, 2015.
- Yue, X., Unger, N., Keenan, T. F., Zhang, X., and Vogel, C. S.: Probing the past 30-year phenology trend of U.S. deciduous forests, *Biogeosciences*, 12, 4693-4709, doi:10.5194/bg-12-4693-2015, 2015.
- Zheng, Y., Unger, N., Barley, M., and Yue, X.: Relationships between photosynthesis and formaldehyde as a probe of isoprene emission, *Atmos. Chem. Phys.*, 15, 8559-8576, doi:10.5194/acp-15-8559-2015, 2015.

1 **Distinguishing the drivers of trends in land carbon fluxes and plant volatile**
2 **emissions over the past three decades**

3
4 X. Yue¹, N. Unger¹, Y. Zheng²

5
6 ¹ School of Forestry and Environment Studies, Yale University, New Haven, Connecticut
7 06511, USA
8 ² Department of Geology and Geophysics, Yale University, New Haven, Connecticut
9 06511, USA

10
11
12
13 *Correspondence to:* X. Yue (xuyueseas@gmail.com)
14
15

Abstract

16
17
18 The terrestrial biosphere has experienced dramatic changes in recent decades. Estimates
19 of historical trends in land carbon fluxes remain uncertain because long-term
20 observations are limited on the global scale. Here, we use the Yale Interactive terrestrial
21 Biosphere (YIBs) model to estimate decadal trends in land carbon fluxes and emissions
22 of biogenic volatile organic compounds (BVOCs) and to identify the key drivers for these
23 changes during 1982-2011. Driven with hourly meteorology from WFDEI (WATCH
24 Forcing Data methodology applied to ERA-Interim data), the model simulates an
25 increasing trend of 297 Tg C a⁻² in gross primary productivity (GPP) and 185 Tg C a⁻² in
26 the net primary productivity (NPP). CO₂ fertilization is the main driver for the flux
27 changes in forest ecosystems, while meteorology dominates the changes in grasslands
28 and shrublands. Warming boosts summer GPP and NPP at high latitudes, while drought
29 dampens carbon uptake in tropical regions. North of 30°N, increasing temperatures
30 induce a substantial extension of 0.22 day a⁻¹ for the growing season; however, this
31 phenological change alone does not promote regional carbon uptake and BVOC
32 emissions. Nevertheless, increases of LAI at peak season accounts for ~25% of the trends
33 in GPP and isoprene emissions at the northern lands. The net land sink shows statistically
34 insignificant increases of only 3 Tg C a⁻² globally because of simultaneous increases in
35 soil respiration. Global BVOC emissions are calculated using two schemes. With the
36 photosynthesis-dependent scheme, the model predicts increases of 0.4 Tg C a⁻² in
37 isoprene emissions, which are mainly attributed to warming trends because CO₂
38 fertilization and inhibition effects offset each other. Using the MEGAN (Model of
39 Emissions of Gases and Aerosols from Nature) scheme, the YIBs model simulates global
40 reductions of 1.1 Tg C a⁻² in isoprene and 0.04 Tg C a⁻² in monoterpene emissions in
41 response to the CO₂ inhibition effects. Land use change shows limited impacts on global
42 carbon fluxes and BVOC emissions, but there are regional contrasting impacts over
43 Europe (afforestation) and China (deforestation).
44

Xu Yue 10/6/15 1:41 PM

Deleted: In contrast, driven with alternative meteorology from MERRA (Modern Era-Retrospective Analysis), the model predicts significant increases of 59 Tg C a⁻² in the land sink due to strengthened uptake in the Amazon.

51 **1 Introduction**

52

53 The terrestrial biosphere interacts with the atmosphere through photosynthesis and
54 biogenic volatile organic compound (BVOC) emissions. Annually, terrestrial ecosystems
55 assimilate ~120 petagrams of carbon (Pg C) from the atmosphere (Beer et al., 2010),
56 most of which reenters atmosphere through respiration and decomposition, resulting in a
57 net global land carbon sink of 2.6 ± 0.7 Pg C a⁻¹ (Le Quere et al., 2009; Sitch et al.,
58 2015). Global BVOC emissions are estimated to be about 1 Pg C per year (Carslaw et al.,
59 2010). These emissions are important precursors of atmospheric oxidants and aerosols,
60 both of which affect surface air quality and exert additional regional and global chemical
61 climate forcings (Scott et al., 2014; Unger, 2014). Observations and simulations have
62 shown significant changes in terrestrial carbon assimilation and BVOC emissions in the
63 past 2-3 decades (Lathiere et al., 2006; Sarmiento et al., 2010; Sindelarova et al., 2014;
64 Sitch et al., 2015). Understanding drivers of these trends is important for the projections
65 of future carbon fluxes, water cycle, air quality, and climatic responses.

66

67 Trends in land carbon assimilation and BVOC emissions are related to the changes in
68 atmospheric CO₂, meteorology, and human land use land cover change perturbations.
69 Elevated CO₂ promotes plant photosynthesis (Ainsworth and Long, 2005) but can
70 directly inhibit isoprene productions (Arneth et al., 2007). Warming accelerates both
71 carbon uptake and BVOC emissions when temperature is not above the thermal optimum
72 (25-30 °C for photosynthesis and 35-40 °C for isoprene emission) for ecosystems that are
73 not water-stressed (Farquhar et al., 1980; Guenther et al., 1993; Piao et al., 2013).
74 Additional warming above thermal optimum may decrease photosynthesis but still
75 promote respiration, reducing net carbon uptake by plants (Liang et al., 2013). Increased
76 temperatures also indirectly influence carbon exchange and BVOC emissions through the
77 extension of growing season (Piao et al., 2007). Drought decreases gross primary
78 productivity (GPP) and net primary productivity (NPP) (Zhao and Running, 2010), but
79 may temporally enhance isoprene emissions (Monson et al., 2007). Land use change
80 affects the regional carbon budget and BVOC emissions through either additional

81 emissions or land cover changes due to deforestation, forest management, and
82 agricultural activities (Lathiere et al., 2006; Houghton, 2010).

83

84 Estimates of recent decadal global trends in the land carbon budget and BVOC emissions
85 are limited and uncertain due to the lack of observations. The earliest site-level
86 measurements of land carbon fluxes were set up in the 1990s (Wofsy et al., 1993). The
87 flux tower data sets provide long-term records of regional carbon exchange with high
88 precision but low spatial representation. In contrast, satellite products, such as GPP and
89 NPP retrievals from the Moderate Resolution Imaging Spectroradiometer (MODIS)
90 (Zhao et al., 2005) and isoprene emissions based on tropospheric formaldehyde columns
91 from the Global Ozone Monitoring Experiment (Palmer et al., 2006), improve the spatial
92 coverage but usually are available for only a relatively short time period (months to
93 several years) and suffer from systematic biases when compared with ground
94 measurements (e.g., Heinsch et al., 2006; Marais et al., 2012). Terrestrial biosphere
95 models, evaluated with both site-level and satellite-based observations, are useful tools to
96 estimate trends and attribute drivers of changes in land carbon fluxes and BVOC
97 emissions (e.g., Mao et al., 2013; Stavrakou et al., 2014; Sitch et al., 2015).

98

99 In this study, we use the Yale Interactive Terrestrial Biosphere Model (YIBs, Yue and
100 Unger, 2015) driven with long-term reanalysis meteorology to study the global trends of
101 land carbon fluxes and BVOC emissions over the past three decades. The YIBs model is
102 a process-based vegetation model including complete land carbon cycle (photosynthesis,
103 plant/soil respiration, carbon allocation, and tree growth), plant phenology (Yue et al.,
104 2015), and two independent schemes of BVOC emissions (Zheng et al., 2015). Simulated
105 carbon fluxes has been fully validated with carbon fluxes from 145 flux tower sites and
106 multiple satellite products (Yue and Unger, 2015). The major goals of this study are to
107 identify: (1) the dominant drivers of the 30-year trends in carbon fluxes and BVOC
108 emissions from elevated CO₂, changes in meteorology (temperature, radiation, and soil
109 moisture), and human land use change; (2) the feedback of biosphere, including changes
110 in phenology and leaf area index (LAI), to the trends of land carbon uptakes and BVOC

Unknown

Field Code Changed

Unknown

Field Code Changed

Xu Yue 10/6/15 1:41 PM

Deleted: In this study, we use the well-validated Yale Interactive Terrestrial Biosphere Model (YIBs, Yue and Unger, 2015) driven with long-term reanalysis meteorology to study the global trends of land carbon fluxes and BVOC emissions over the past three decades. We compare the simulated trends with satellite observations where available (Jeong et al., 2011; Zhu et al., 2013) and multi-model ensemble estimates (e.g., Piao et al., 2013; Sitch et al., 2015). The major goals of this study are to quantify: (1) the spatial distribution of global trends in carbon fluxes and BVOC emissions during 1982-2011; (2) the dominant drivers of these trends from elevated CO₂, changes in meteorology (temperature, radiation, and soil moisture), and human land use change; (3) the feedback of biosphere, including changes in phenology and leaf area index (LAI), to the land carbon uptakes and BVOC emissions; and (4) the discrepancies in BVOC trends due to application of different isoprene emission schemes. To assess uncertainties due to the meteorological forcings (Poulter et al., 2011), we apply two independent reanalysis datasets as input and compare the corresponding model results. This study does not assess wildfire emissions because no significant global trends have been predicted with the state-of-art terrestrial models (Sitch et al., 2015). In the next section, we describe the physical processes in the model and the simulations performed for trend driver attribution. Section 3 presents the simulated global distribution and associated drivers of the changes in land carbon fluxes and BVOC emissions during the past three decades. Section 4 discusses the observational uncertainties and the model sensitivities. The last section summarizes the derived trends. .

152 | emissions; and (3) the discrepancies in BVOC trends due to application of different
153 | isoprene emission schemes.

154 |

155 |

156 | **2 Data and methods**

157 |

158 | **2.1 Observations and benchmark products**

159 |

160 | We use long-term global measurements of LAI, GPP, and NPP to validate the simulated
161 | trends. The LAI dataset for 1982-2011 is retrieved based on the Normalized Difference
162 | Vegetation Index (NDVI) from Global Inventory Modeling and Mapping Studies
163 | (GIMMS) with 1/12 degree resolution and a 15-day interval (Zhu et al., 2013). We also
164 | use LAI data for 2000-2011 from the MODIS (<http://modis.gsfc.nasa.gov/>). GPP
165 | benchmark products of 1982-2011 are upscaled from the FLUXNET eddy covariance
166 | measurements using an ensemble of regression trees (Jung et al., 2009). As a comparison,
167 | we also use the GPP and NPP datasets for 2000-2011 from the MODIS, which have been
168 | developed based on remote sensing of biome parameters and assimilated meteorology
169 | (Zhao et al., 2005). All the datasets are interpolated to the monthly interval at the 1°×1°
170 | off-line YIBs model resolution.

171 |

172 | **2.2 Model**

173 |

174 | The YIBs model is a process-based terrestrial vegetation model that simulates the land
175 | carbon budget and dynamic tree growth (Yue and Unger, 2015). The model adapts
176 | routines from the mature TRIFFID (Cox, 2001) and CASA (Schaefer et al., 2008) models
177 | with special updates in the parameterizations of ozone vegetation damage (Yue and
178 | Unger, 2014), plant phenology (Yue et al., 2015), and the photosynthesis-dependent
179 | isoprene emission (Unger et al., 2013). The model simulates carbon uptake for 9 plant
180 | functional types (PFTs) including tundra, C3/C4 grass, shrubland, deciduous broadleaf
181 | forest (DBF), ENF evergreen needleleaf forest (ENF), evergreen broadleaf forest (EBF),
182 | and C3/C4 cropland. The vegetation biophysics calculates leaf-level photosynthesis using

Xu Yue 10/6/15 1:41 PM

Deleted: datasets

Xu Yue 10/6/15 1:41 PM

Deleted: a biosphere model

185 the well-established Farquhar scheme (Farquhar et al., 1980; von Caemmerer and
186 Farquhar, 1981) and the stomatal conductance model of Ball and Berry (Collatz et al.,
187 1991). The canopy radiative transfer scheme computes direct and diffuse
188 photosynthetically active radiation (PAR) for sunlit and shaded regions for an adaptive
189 number of layers. The leaf photosynthesis is then integrated over all canopy layers to
190 generate the GPP.

191

192 Part of the assimilated carbon is used for maintenance and growth respiration, and the
193 rest is allocated among different pools for plant development. The model calculates
194 phenology for deciduous forests using cumulative temperature summation with additional
195 constraints from chilling and photoperiod (Yue et al., 2015). The phenology of shrubland
196 and grassland is jointly determined by the temperature- and drought-dependent metrics.
197 The LAI is then updated daily based on phenology and the net carbon assimilation. The
198 soil respiration scheme considers carbon flows among 12 biogeochemical pools,
199 including 3 live pools and 9 dead pools. The land carbon source or sink is calculated as
200 the difference between the net carbon assimilation and soil respiration.

201

202 The YIBs model incorporates two independent leaf-level isoprene emission schemes
203 embedded within the exact same host model framework (Zheng et al., 2015). The
204 photosynthesis-based (PS_BVOC) isoprene scheme calculates emissions based on the
205 electron transport-limited photosynthesis rate, canopy temperature, and intercellular CO₂
206 concentrations (Arneeth et al., 2007; Unger et al., 2013). The Model of Emissions of
207 Gases and Aerosols from Nature (MEGAN) scheme applies commonly used leaf-level
208 empirical functions of light and canopy temperature. Both schemes implement CO₂
209 inhibition effects on BVOC emissions parameterized as a reciprocal empirical function of
210 intercellular [CO₂] following the observations from Possell et al. (2005). For
211 monoterpene emissions, the YIBs model applies the same temperature-dependent scheme
212 as Lathiere et al. (2006) but with CO₂-inhibition effects. The leaf-level BVOC emissions
213 are integrated over the multiple canopy layers following the same approach as GPP to
214 obtain the total canopy-level emissions.

215

216 YIBs can be used in three different configurations with increasing complexity: (1) off-
217 line local site level, which is driven with hourly measurements of CO₂ concentrations and
218 meteorology at flux tower sites; (2) off-line global forced with spatially uniform but
219 annually updated CO₂ concentrations and hourly gridded reanalysis meteorology; (3) on-
220 line coupled to the NASA ModelE2 driven with simulated meteorology by the GCM
221 every half hour. At the site level, YIBs simulates reasonable seasonality (correlation
222 coefficient $R > 0.8$) of GPP at 121 out of 145 flux-tower sites with biases in magnitude
223 ranging from -19 to 7 % depending on PFTs. On the global scale, the offline model
224 simulates an annual GPP of 125 ± 3 Pg C and net ecosystem exchange (NEE) of $-2.5 \pm$
225 0.7 Pg C for 1982-2011, with seasonality and spatial distribution consistent with both
226 satellite observations and benchmark synthesis products (Yue and Unger, 2015).
227 However, the model does not include a fully coupled carbon-nitrogen cycle, which may
228 overestimate CO₂ fertilization effects. In addition, phenology of evergreen trees is set to
229 constant value of 1, leading to underestimation of phenological feedbacks to flux trends.
230 In this study, we use the (2) off-line global version of the model, which is driven with
231 global meteorology reanalysis data and observed CO₂ concentrations.

232

233 2.3 Simulations

234

235 We apply observed historical atmospheric CO₂ concentrations from the fifth assessment
236 report (AR5) of the Intergovernmental Panel on Climate Change (IPCC) (Meinshausen et
237 al., 2011). We apply an annually-varying historical transient land cover dataset (Oleson et
238 al., 2013), which is developed based on a combination of remote sensing data from both
239 MODIS (Hansen et al., 2003) and the Advanced Very High Resolution Radiometer
240 (AVHRR) (Defries et al., 2000), and with land use change from Hurtt et al. (2011). We
241 use hourly meteorological variables for 1980-2011 from the WATCH Forcing Data
242 methodology applied to ERA-Interim data (WFDEI, Weedon et al., 2014). The WFDEI
243 reanalysis is an update of the WATCH Forcing Data (WFD), which is developed based
244 on the European Centre for Medium-range Weather Forecasts (ECMWF) ERA-40
245 reanalysis (Uppala et al., 2005). Meteorological variables applied include surface air
246 temperature, specific humidity, wind speed, surface pressure, total PAR, and soil

Xu Yue 10/6/15 1:41 PM

Deleted: All of the three configurations have been fully validated with carbon fluxes from 145 flux tower sites and multiple satellite products (Yue and Unger, 2015).

Xu Yue 10/6/15 1:41 PM

Deleted: two independent reanalysis datasets as a comparison. The first is

Xu Yue 10/6/15 1:41 PM

Deleted: . The other is the Global Modeling and Assimilation Office (GMAO) Modern Era-Retrospective Analysis (MERRA) data set, which is generated with the GEOS-5 atmospheric general circulation model (AGCM) by assimilating both *in situ* and remote sensing observations (Rienecker et al., 2011). The MERRA-land product is a supplemental and improved set of land surface hydrological fields for MERRA (Reichle et al., 2011).

264 temperature and wetness. All of the forcing data are interpolated to the $1^{\circ}\times 1^{\circ}$ model
265 resolution at the hourly interval.

266

267 We perform 10 sensitivity simulations to distinguish driving factors for the changes in
268 land carbon fluxes and BVOC emissions in the past 3 decades (Table 1). The control
269 simulation (CO2_MET_LUC) uses interannually-varying meteorology, [CO₂], and land
270 cover for 1980-2011. The CO2_MET run is the same as the control simulation but
271 prescribes land cover at the year 1980. Three single-factor runs prescribe most boundary
272 conditions at the year 1980 but allow the interannual variations of [CO₂] (CO2_ONLY),
273 land cover (LUC_ONLY), and meteorology (MET_ONLY) respectively. Results from
274 these runs are compared with that of control simulation to determine the dominant drivers
275 of simulated trends. To understand the impact of individual meteorological variables,
276 three additional runs are performed with fixed (or recycled) [CO₂], land cover, and all
277 meteorology at year 1980 but one field varying for 1980-2011 each time, including
278 temperature (TEMP_ONLY), PAR (PAR_ONLY), and soil wetness (SOILW_ONLY).
279 Finally, two runs are performed to examine feedback of biospheric changes. LAI_ONLY
280 prescribes all boundary conditions at the starting year 1980 but implements the year-to-
281 year LAI simulated by the control run. PHEN_ONLY also prescribes all forcings at the
282 starting year except for the year-to-year phenology from control simulation. All
283 simulations are initialized following the same spin up process (Yue and Unger, 2015) and
284 are integrated for 1980-2011.

285

286

287 3 Results

288

289 3.1 Drivers of trends in LAI

290

291 Observations show an increasing trend of LAI on most of vegetated continents, especially
292 in Europe, northern and eastern Asia, central Africa, and southeastern U.S. in the past 3
293 decades (Fig. 1a). The simulation with year-to-year [CO₂], land cover, and meteorology
294 reproduces the magnitude of trend in Europe and the sign of trend in northern Asia,

Xu Yue 10/6/15 1:41 PM

Deleted: with WFDEI reanalysis

Xu Yue 10/6/15 1:41 PM

Deleted: (Yue and Unger, 2015) and are integrated for 1980-2011. To assess uncertainties due to meteorology, we perform 7 other sensitivity runs driven with MERRA reanalysis. These MERRA simulations follow the same designs as that with WFDEI (Table 1) but omit runs of CO2_MET, LAI_ONLY and PHEN_ONLY. In the following sections, we discuss results of 1982-2011 driven with WFDEI reanalysis. Results forced with MERRA reanalysis are used in the comparison to understand the simulation uncertainties due to the historical meteorology changes

Xu Yue 10/6/15 1:41 PM

Deleted: Trends

310 eastern U.S., central Asia, and Australia (Fig. 1b). The model predicts negative changes
311 in central Africa, western U.S., eastern Asia, and the east of South America, which are
312 inconsistent with satellite observations. These negative trends are mainly contributed by
313 the changes in meteorology (Fig. 1e), except for that in East Asia where land cover
314 changes due to human activities result in the decline of LAI (Fig. 1f). Without the land
315 use perturbation, the negative LAI trend in East Asia is weakened and the prediction is
316 closer to observations (Fig. 1c). For the individual drivers, CO₂ fertilization leads to
317 widespread increases in LAI (Fig. 1d), meteorology causes dipole changes on most
318 continents (Fig. 1e), and land use change generally results in negative trends (Fig. 1f).
319 Regionally, simulation CO₂_MET_LUC shows a positive trend of 0.0035 m² m⁻² a⁻¹ in
320 Europe (Table 2), close to the observed value of 0.0049 m² m⁻² a⁻¹ (Fig. 1a). In other
321 areas, simulated LAI trends are either underestimated (by 87% in Amazon, 78% in North
322 America, and 48% in Central Africa) or opposite in sign (East Asia and Indonesia)
323 compared to observations. Such inconsistencies indicate the limit of model simulations,
324 but may also in part result from the uncertainties in the satellite measurements (see
325 section 4.1).

326

327 | 3.2 Drivers of trends in land carbon fluxes

328

329 Predicted GPP and NPP trends show similar spatial pattern as that of LAI (Figs. 2a and
330 | 2c). However, regional trends are all positive in the main continents and on the global
331 scale (Tables 2 and 3). Tropical areas are experiencing maximum changes, especially in
332 Central Africa (GPP by 83.3 Tg C a⁻² and NPP by 51.7 Tg C a⁻²) and the Amazon (52.7
333 and 27.1 Tg C a⁻²). In the Northern Hemisphere (NH), changes are significant in Europe
334 (53.4 and 33.2 Tg C a⁻²), East Asia (42.4 and 27.2 Tg C a⁻²), and North America (13.6
335 | and 9.7 Tg C a⁻²). 30-year historical observations of GPP and NPP are not available.
336 Therefore, we compare YIBs predictions with MODIS land carbon fluxes over the more
337 recent period of 2000-2011 (Fig. 3). Different from the 30-year trend, land carbon fluxes
338 over the recent decade show negative trends in southeastern U.S., southern Africa,
339 eastern Australia, and central and northern Asia (Figs. 3a and 3c). Most of these changes

Xu Yue 10/6/15 1:41 PM

Deleted: Trends

Xu Yue 10/6/15 1:41 PM

Deleted: 2b

Xu Yue 10/6/15 1:41 PM

Deleted: On the larger domain, the YIBs model predicts NPP trends of 67.4 Tg C a⁻² in northern land (25-90°N) and 98.1 Tg C a⁻² in tropical land (15°S-25°N), similar to the ensemble estimates of 63 ± 22 and 102 ± 34 Tg C a⁻² for 1990-2009 based on 9 terrestrial biosphere models (Sitch et al., 2015). However, the simulated NPP trend is only 19.8 Tg C a⁻² in southern land (15-90°S), much lower than the ensemble mean value of 53 ± 31 Tg C a⁻² in Sitch et al. (2015). .

... [1]

354 are consistent with the MODIS observations (except for the U.S., Figs. 3b and 3d) and
355 are attributed to the drought tendency in the past decade (Zhao and Running, 2010).

356
357 For the 30-year trend, both CO₂ and meteorology are playing important roles (Figs. 2b
358 and 2d). CO₂ fertilization dominates the GPP and NPP trends of tropical forests in the
359 Amazon, central Africa, and Indonesia, and ENF and DBF in boreal North America,
360 eastern Europe, and central and northern Asia. Land use change plays a limited role in
361 land carbon cycle flux trends over the past 3 decades, except for some areas in northern
362 Africa. Meteorological forcing drives changes in land carbon fluxes for tundra in
363 subarctic regions, C3 grasslands in the central U.S. and southern Africa, C4 grasslands in
364 central Africa and the east of South America, and shrublands in Australia and southern
365 Asia. Soil wetness plays the dominant role in the tropical and subtropical areas (Fig. 4b).
366 The drought tendency in the western U.S., central Africa, and the east of South America
367 (Fig. S1d) results in the regional decline of land carbon fluxes (Fig. 4a). In contrast, the
368 increasing wetness in the northern Amazon and southern Africa leads to the enhancement
369 of regional GPP. Warming is the main cause for the GPP trends over the subarctic areas
370 (Fig. 4b). Contribution of PAR is limited, except for some areas in the eastern Europe.

371
372 The simulated net ecosystem productivity (NEP) shows weaker trends compared with
373 GPP and NPP (Fig. 2e), because NEP is offset by the significant trends in heterotrophic
374 respiration (Rh) (Table 2). Regionally, the YIBs model predicts enhanced net land carbon
375 uptake in boreal North America, northern Asia, and southern Africa but reduced NEP in
376 the central U.S., the Amazon, central Africa, eastern Europe, and East Asia. The
377 simulated global NEP trends (Fig. 5d) are in broad agreement with the comprehensive
378 bottom-up estimates by Pan et al. (2011), who found slightly decreasing net carbon
379 uptake by global established forests (without human perturbations in the tropics but with
380 afforestation in subtropical areas) in 2000-2007 relative to that in 1990-1999. Attribution
381 analysis shows that the NEP trends are mainly driven by the changes in meteorological
382 forcings (Fig. 2f), because CO₂ fertilization enhances both NPP and Rh with similar
383 magnitude (Fig. 5).

384

Xu Yue 10/6/15 1:41 PM

Deleted: 2d

Xu Yue 10/6/15 1:41 PM

Deleted: 2e

Xu Yue 10/6/15 1:41 PM

Deleted: Meteorological forcing drives changes in land carbon fluxes for tundra in subarctic regions, C3 grasslands in the central U.S., southern Africa, and the southern tips of South America, C4 grasslands in central Africa and the east of South America, and shrublands in Australia and southern Asia.

Xu Yue 10/6/15 1:41 PM

Deleted: -

... [2]

Xu Yue 10/6/15 1:41 PM

Deleted: meteorology-induced GPP trends (Fig. 4).

Xu Yue 10/6/15 1:41 PM

Deleted: 4c

Xu Yue 10/6/15 1:41 PM

Deleted: S2d

Xu Yue 10/6/15 1:41 PM

Deleted: 4c). Contribution of PAR is limited, except for some areas in the eastern Europe. Driven with MERRA reanalysis, simulated GPP shows similar trends as that with WFDEI reanalysis, except for tropical areas where MERRA-forced runs exhibit stronger magnitude (Fig. 4b). The cooling tendency of MERRA temperature in the Amazon (Fig. S3a) increases regional GPP, because the climatological temperature is higher than the optimal temperature of 25°C for the light-saturated photosynthesis (Yue and Unger, 2015). The large reductions in soil wetness in central Africa (Fig. S3d) result in the decline of GPP (Fig. 4b). In the western U.S., predictions with MERRA show smaller reductions in GPP relative to those using WFDEI, because the drought tendency is weaker in the former dataset (Figs. S2d and S3d).

Xu Yue 10/6/15 1:41 PM

Deleted: 2c

Xu Yue 10/6/15 1:41 PM

Deleted: All these changes are consistent with the ensemble estimates based on 9 terrestrial models for 1990-2009 (Sitch et al., 2015). On the larger domain, the YIBs model predicts NEP trends of 2.0 Tg C a⁻² in northern land, 1.0 Tg C a⁻² in tropical land, and -0.3 Tg C a⁻² in southern land, much smaller in magnitude compared with the -2.0 ± 12, 36.0 ± 13, and 21 ± 17 Tg C a⁻² estimated by S... [3]

Xu Yue 10/6/15 1:41 PM

Deleted: A similar conclusion is achieved using MERRA reanalysis (Fig. S1f).

447 On the global scale, GPP, NPP, and Rh increase respectively by 298, 185, and 181 Tg C
448 | a⁻² in the past 3 decades (Table 3). The long-term trends of carbon fluxes are mainly
449 driven by CO₂ fertilization, while the interannual variability is related to meteorological
450 forcings (Fig. 5). Warming alone decreases GPP especially in tropical forests (not shown)
451 but increases autotrophic respiration (Ra), leading to global reductions of 56 Tg C a⁻² in
452 NPP and 10 Tg C a⁻² in NEP (Table 3). Drought alone strongly decreases GPP, especially
453 for tropical grassland and shrubland (Fig. 4), leading to reductions of 51 Tg C a⁻² in NPP
454 and 13 Tg C a⁻² in NEP. Trends in PAR do not affect GPP and NPP, but may decrease
455 NEP by 23 Tg C a⁻² because soil respiration is slowly increasing to reach the equilibrium.
456 Land use change has very limited impacts on the trends of carbon fluxes, though it
457 | induces relatively large reductions in NEP (Table 3).

458

459 | 3.3 Drivers of trends in BVOC emissions

460

461 Simulated isoprene emission trends are sensitive to the choice of modeling scheme. With
462 the PS_BVOC scheme, global isoprene emissions increase by 0.4 Tg C a⁻² during 1982-
463 2011. Large enhancements are predicted in central Africa (0.25 Tg C a⁻²) and Europe
464 (0.16 Tg C a⁻²), while moderate reductions are found in the western U.S., eastern South
465 America, and East Asia (Fig. 6a). Drought accounts for the decline of isoprene emissions
466 in the U.S. and South America, but land use change is the main driver for the reductions
467 | in East Asia (Fig. 6b). Increasing [CO₂] promotes photosynthesis but meanwhile inhibits
468 BVOC emissions, leading to offsetting CO₂ effects on isoprene. Consequently, the global
469 | isoprene emission is mainly driven by meteorological changes (Fig. 6b). In contrast,
470 using MEGAN scheme, the YIBs model simulates a global reduction of 1.1 Tg C a⁻² for
471 | isoprene emissions (Fig. 6c). Strong declines are found in the tropical rainforest, for
472 example in the Amazon (-0.43 Tg C a⁻²), central Africa (-0.14 Tg C a⁻²), and Indonesia (-
473 | 0.16 Tg C a⁻²) (Fig. 6c). The MEGAN scheme is sensitive to both light and temperature
474 (Guenther et al., 1995). The strong positive brightening trends in PAR in Europe (Fig.
475 | S1b) promote isoprene emissions there. The positive impacts of NH warming (Fig. S1a)
476 are compensated by CO₂ inhibition, leading to small changes in isoprene emissions (Fig.
477 | 6c). In the tropical areas, where trends of temperature and PAR are limited, CO₂

Xu Yue 10/6/15 1:41 PM

Deleted: The ensemble estimates by Sitch et al. (2015) yield a NPP trend of 218 ± 76 Tg C a⁻² and Rh trend of 160 ± 53 Tg C a⁻². The lower NPP trend in YIBs is mainly attributed to the smaller enhancement in southern land due to the negative trends in South America (Fig. 2b). The higher Rh trend in YIBs is a result of the larger enhancement in tropical forests due to the increased litterfall following CO₂ fertilization (not shown).

Xu Yue 10/6/15 1:41 PM

Deleted: In this study, we do not include land-use-induced carbon emissions, which result in a net land carbon source (Ciais et al., 2013).

Xu Yue 10/6/15 1:41 PM

Deleted: Trends

Xu Yue 10/6/15 1:41 PM

Deleted: 6d

Xu Yue 10/6/15 1:41 PM

Deleted: 6d

Xu Yue 10/6/15 1:41 PM

Deleted: 6b

Xu Yue 10/6/15 1:41 PM

Deleted: 6b

Xu Yue 10/6/15 1:41 PM

Deleted: S2b

Xu Yue 10/6/15 1:41 PM

Deleted: S2a

Xu Yue 10/6/15 1:41 PM

Deleted: 6b

500 inhibition results in strong reductions of BVOC emissions. Monoterpene emissions show
501 a global reduction of 0.04 Tg C a⁻² over the past 3 decades (Fig. 6e).

502

503

504

505 3.4 Feedback of biospheric changes to the trends

506

507 Due to the changing climate and CO₂ fertilization, the biosphere is experiencing
508 significant changes in the past 3 decades. The most evident alterations include LAI
509 changes in peak season and phenological changes in growing and falling seasons. In this
510 section, we explore the feedback of these biospheric changes to the carbon uptake and
511 BVOC emissions.

512

513 3.4.1 Impacts of LAI changes

514

515 Sensitivity run LAI_ONLY retains the trends in LAI but prescribes other forcings. In this
516 simulation, trends in GPP (Fig. S2a) and NPP (Fig. S2c) generally follow that in LAI
517 (Fig. 1b), but with smaller magnitude relative to those in control simulations (Figs. 2a
518 and 2c). LAI in the north of 30°N shows widespread increases in both observations and
519 simulations (Figs. 1a and 1b). Over these northern lands, the unit change in leaf area
520 leads to enhancement of regional GPP by 32 Pg C a⁻¹, much lower than the response of
521 116 Pg C a⁻¹ LAI⁻¹ for the simulation including CO₂ fertilization and climate forcings
522 (Fig. 7a). In the tropical areas, both positive and negative LAI trends are predicted due to
523 the competition between CO₂ fertilization and drought effects (Fig. 1). As a result, LAI-
524 induced GPP and NPP changes show patchy distributions at tropics (Fig. S2a and S2c),
525 leading to moderate changes in the global carbon assimilations (Table 3).

526

527 Trends in isoprene emission (calculated with the PS_BVOC scheme) also follow that of
528 LAI, except that leaf expansion results in decreased emissions at high latitudes (~60°N,
529 Fig. S2e). The cause for such inconsistency is unclear, but might be because the denser
530 leaves reduce radiation penetrating to lower canopy layers. Such impact would only

Xu Yue 10/6/15 1:41 PM

Deleted: 6c). Similar conclusions are achieved with the MERRA reanalysis (Fig. S4

Xu Yue 10/6/15 1:41 PM

Moved down [1]: investigated isoprene emissions over Asia during 1979-2012 using the MEGAN scheme and taking into account both climate and land-use changes. Their results showed widespread increases in the emissions over China but moderate decreases in Indonesia. In contrast, the YIBs model with the MEGAN scheme simulates widespread reductions in the same areas for 1980-2011 (Fig.

Xu Yue 10/6/15 1:41 PM

Deleted: 6b

Xu Yue 10/6/15 1:41 PM

Moved down [2]:). The discrepancies between studies are accounted for by differences in the drivers including land ... [5]

Xu Yue 10/6/15 1:41 PM

Deleted: We compare our results with previous estimates of long-term BVOC ... [4]

Xu Yue 10/6/15 1:41 PM

Deleted: The YIBs model is driven with land cover data from Hurtt et al. (2011), whi ... [6]

Xu Yue 10/6/15 1:41 PM

Moved down [3]: shows an increasing trend in southeast China (c.f. their Fig. ... [7]

Xu Yue 10/6/15 1:41 PM

Deleted: S2b), leading to a reduction in isoprene emissions. The WFDEI surfac ... [8]

Xu Yue 10/6/15 1:41 PM

Moved down [4]: reported a global increase of 4.5 Tg C a⁻² for 1995-2006 ... [9]

Xu Yue 10/6/15 1:41 PM

Deleted: The YIBs result is consistent with a recent study by Sindelarova et al. (2014)

Xu Yue 10/6/15 1:41 PM

Moved down [5]: , who reported a decreasing trend of ~1.2 Tg C a⁻² for g ... [10]

Xu Yue 10/6/15 1:41 PM

Deleted: S5a

Xu Yue 10/6/15 1:41 PM

Deleted: S5c

Xu Yue 10/6/15 1:41 PM

Deleted: 2b

Xu Yue 10/6/15 1:41 PM

Deleted: S5a

Xu Yue 10/6/15 1:41 PM

Deleted: S5c

Xu Yue 10/6/15 1:41 PM

Deleted: S5e

626 affect BVOC emissions at high latitudes because PAR is usually limiting near subarctic
627 areas. In most of the subtropical areas, increased LAI leads to enhanced isoprene
628 emissions. On average, unit change in LAI at north of 30°N leads to enhanced isoprene
629 emissions by 43 Tg C a⁻², only 25% of the magnitude in simulation CO2_MET (Fig. 7b).
630 A similar ratio of 23% is achieved for MEGAN isoprene emissions. These results are
631 consistent with that for GPP (Fig. 7a), suggesting that CO₂ fertilization and
632 meteorological changes are the main drivers for the changes in carbon uptake and BVOC
633 emissions, even over the northern lands where the most evident changes in LAI are
634 observed.

635

636 3.4.2 Impacts of phenological changes

637

638 Plant phenology, which is the timing of budburst and leaf fall, is closely related to
639 temperature, moisture, and photoperiod and thus is experiencing significant changes in
640 the past decades following climate change (Jeong et al., 2011; Keenan et al., 2014;
641 Buitenwerf et al., 2015; Yue et al., 2015). Extension of the growing season has the
642 potential to promote carbon uptake of forests (e.g., Piao et al., 2007; Richardson et al.,
643 2009). Yet such inference requires careful interpretation because the phenological
644 changes are usually accompanied with warming and elevated [CO₂], both of which are
645 also contributing to the enhancement of carbon fluxes. Phenological changes are also
646 expected to affect BVOC emissions, however, such investigations are still missing
647 (Richardson et al., 2013). With the YIBs model, we evaluate the impacts of the growing
648 season extension on both carbon uptake and BVOC emissions by isolating long-term
649 phenological trends from changes in temperature and [CO₂].

650

651 The YIBs model simulates advanced spring and delayed autumn over most areas in NH
652 (Fig. S3). Budburst dates advance on average by 0.16 days a⁻¹ in Europe and 0.15 days a⁻¹
653 in East Asia (Table 2), but with moderate changes or even delays in northwestern Asia
654 and eastern Siberia (Fig. S3a). Spring is earlier by 0.14 days a⁻¹ in eastern U.S. while
655 delayed by 0.15 days a⁻¹ in northwestern U.S. and southeastern Canada, leading to a
656 minor advance of 0.01 days a⁻¹ over North America. Dormancy onset dates are largely

Xu Yue 10/6/15 1:41 PM

Deleted: S6

Xu Yue 10/6/15 1:41 PM

Deleted: S6a

659 delayed in eastern Europe and northwestern Asia ($\sim 0.3 \text{ day a}^{-1}$), western U.S. ($\sim 0.1 \text{ day a}^{-1}$), boreal Canada ($\sim 0.1 \text{ day a}^{-1}$), and northeastern China ($\sim 0.1 \text{ day a}^{-1}$) (Fig. S3b).
660
661 Advanced autumn ($\sim 0.1 \text{ day a}^{-1}$) is predicted in northern Asia. Most of these changes are
662 consistent with observations from remote sensing data (Jeong et al., 2011), except for
663 some discrepancies in the magnitude. The predicted phenological trends mainly follow
664 the long-term changes of surface air temperature, especially that in April (for spring) and
665 September (for autumn) (Fig. S4). Sensitivity tests without chilling requirement and
666 photoperiod limit show similar changes (Yue et al., 2015), suggesting that temperature
667 changes dominantly drive the trends of forest phenology in the past 3 decades.

668

669 On average, the YIBs model simulates advanced budburst by 0.12 day a^{-1} and delayed
670 dormancy onset by 0.09 day a^{-1} at north of 30°N in the past 3 decades (Figs. 8a and 8b).
671 Observations based on remote sensing greenness show trends of -0.11 day a^{-1} for onset
672 and 0.25 day a^{-1} for offset during 1990-2009 (Zhu et al., 2013). An ensemble prediction
673 based on 9 terrestrial models yields an advance of $0.08 \pm 0.13 \text{ day a}^{-1}$ for onset and a
674 delay of $0.22 \pm 0.1 \text{ day a}^{-1}$ for offset (Sitch et al., 2015). Our predictions are in broad
675 agreement with these estimates though the autumn delay is less, likely because the
676 positive trend of offset is weaker for the recent decade (Jeong et al., 2011).

677

678 We plot the annual total GPP and isoprene emissions at north of 30°N against the length
679 of growing season for 1982-2011 (Figs. 8c and 8d). In the CO2_MET run, the 1-day
680 extension is correspondent to increases of 0.17 Pg C a^{-1} in GPP and 0.34 Tg C a^{-1} in
681 isoprene emissions. If only temperature is allowed to vary, the phenological trend
682 remains the same while the increases of GPP and isoprene emissions are largely
683 weakened. In the TEMP_ONLY run, the 1-day extension in growing season is
684 accompanied by increases of 0.05 Pg C a^{-1} in GPP and 0.25 Tg C a^{-1} in isoprene
685 emissions. The changes in BVOC emissions are not as dramatic as those of GPP because
686 CO₂ has both enhancing and suppressing impacts on the former. If we further exclude
687 temperature effects (PHEN_ONLY run), GPP increases only by 0.01 Pg C a^{-1} while
688 isoprene emissions decrease by 0.1 Tg C a^{-1} , both of which are not statistically
689 significant, suggesting that the phenological change alone does not promote either GPP

Xu Yue 10/6/15 1:41 PM

Deleted: S6b

Xu Yue 10/6/15 1:41 PM

Deleted: S7

692 or isoprene emissions. There are two reasons for this apparent contradiction. First, the
693 extension of the growing season occurs in shoulder months, usually in May and
694 September, when both GPP and BVOC emissions and their changes are much smaller
695 compared to that in peak months (Fig. S5). Second, phenological changes are not uniform
696 in space. As Fig. S3 shows, both positive and negative changes are predicted for budburst
697 and dormancy onset dates. Such spatial inhomogeneity, in combination with the
698 discrepancies in regional vegetation types and meteorological conditions, result in varied
699 responses in GPP (Fig. S2b) and isoprene emissions (Fig. S2f).

700
701 Plant phenology at lower latitudes (30°S-30°N) is also experiencing dramatic changes,
702 though such changes are diverse in phase, magnitude, or both (Buitenwerf et al., 2015).
703 In the model, tropical phenology is mainly driven by soil wetness and as a result exhibits
704 large changes in the past 3 decades (not shown). These changes lead to a reduction of 42
705 Tg C a⁻¹ in GPP at the tropics (Fig. S2b), which accounts for 14% of global GPP trend
706 but with the opposite sign (Table 3), suggesting additional inhibition of drought on
707 carbon cycle. A similar conclusion applies for BVOC emissions (Fig. S2f), though
708 experiments suggest that isoprene production has some tolerance to mild drought
709 conditions (e.g., Pegoraro et al., 2006). However, changes in drought-dependent
710 phenology are very uncertain and observations are not available for evaluation. We
711 assume that phenological changes may have larger impacts on both carbon assimilation
712 and BVOC emissions at tropical areas than that at higher latitudes.

713

714

715 4 Discussion

716

717 4.1 Uncertainties in observations

718

719 Terrestrial biosphere modeling is a useful tool to identify drivers of long-term changes in
720 land carbon fluxes. The reliability of simulations is dependent on the availability of
721 observations for model validation. In this study, we use 30-year LAI observations from
722 the LAI3g product (Zhu et al., 2013) and 12-year GPP from MODIS (Zhao et al., 2005),

Xu Yue 10/6/15 1:41 PM

Deleted: S8

Xu Yue 10/6/15 1:41 PM

Deleted: S6

Xu Yue 10/6/15 1:41 PM

Deleted: S5b

Xu Yue 10/6/15 1:41 PM

Deleted: S5f

Xu Yue 10/6/15 1:41 PM

Deleted: S5b

Xu Yue 10/6/15 1:41 PM

Deleted: S5f

729 both of which are remote sensing retrievals, to validate the simulated trends (Figs. 1 and
 730 3). We found the offline global model biases against both fields, especially for LAI (Fig.
 731 1). Such discrepancies may in part result from the uncertainties in measurements
 732 themselves. As a check, we compare the derived LAI trends from LAI3g with retrievals
 733 from MODIS for the overlap period of 2000-2011 (Figs. [S6a](#) and [S6b](#)). Global LAI
 734 significantly increases in LAI3g but show widespread reductions in MODIS, especially
 735 over subtropical areas. Simulated trends (CO2_LUC_MET) are closer to the estimates
 736 with MODIS, especially for the changes in the NH (not shown). Meanwhile, we compare
 737 the derived GPP trends from MODIS with that upscaled from FLUXNET data using [an](#)
 738 [ensemble of regression trees](#) (Jung et al., 2009) for 2000-2011 (Figs. [S6c](#) and [S6d](#)). The
 739 two products show similar trends over most areas except for some discrepancies in
 740 tropical areas and the eastern U.S. Simulated GPP trends match results from Jung et al.
 741 (2009) better than that from MODIS (Fig. 3a). However, we do not use Jung et al. (2009)
 742 to validate simulations for 1982-2011 because the earliest flux tower observations began
 743 only in middle 1990s. The large discrepancies in the observed trends among different
 744 data sets not only indicate the importance of model evaluations with multiple products,
 745 but also put forward the necessity of data inter-comparisons and algorithm improvements
 746 to alleviate uncertainties in observations.

747

748 **4.2 Comparisons with other modeling studies**

749

750 The YIBs model predicts NPP trends of 67.4 Tg C a⁻² in northern land (25-90°N) and
 751 98.1 Tg C a⁻² in tropical land (15°S-25°N), similar to the ensemble estimates of 63 ± 22
 752 and 102 ± 34 Tg C a⁻² for 1990-2009 based on 9 terrestrial biosphere models

753

754 (Sitch et al., 2015). However, the simulated NPP trend is only 19.8 Tg C a⁻² in southern
 755 land (15-90°S), much lower than the ensemble mean value of 53 ± 31 Tg C a⁻² in Sitch et
 756 al. (2015). As for the NEP, the YIBs predicts trends of 2.0 Tg C a⁻² in northern land, 1.0
 757 Tg C a⁻² in tropical land, and -0.3 Tg C a⁻² in southern land, much smaller in magnitude
 758 compared with the -2.0 ± 12, 36.0 ± 13, and 21 ± 17 Tg C a⁻² estimated by Sitch et al.
 759 (2015). However, their predictions are insignificant (p > 0.05) for 9, 5, and 7 out of 9

Xu Yue 10/6/15 1:41 PM

Deleted: S9a

Xu Yue 10/6/15 1:41 PM

Deleted: S9b

Xu Yue 10/6/15 1:41 PM

Deleted: a biosphere model

Xu Yue 10/6/15 1:41 PM

Deleted: S9c

Xu Yue 10/6/15 1:41 PM

Deleted: S9d

Xu Yue 10/6/15 1:41 PM

Deleted: Impacts

Xu Yue 10/6/15 1:41 PM

Formatted: Font:Not Bold

Xu Yue 10/6/15 1:41 PM

Moved down [6]: CO₂ effects .
 Similar to the multi-model ensemble predictions

Xu Yue 10/6/15 1:41 PM

Deleted: (Sitch et al., 2015)

771 models in the northern, tropical, and southern land respectively, suggesting that the
772 strengthening uptake by terrestrial ecosystem is not robust.

773
774 Stavrakou et al. (2014) investigated isoprene emissions over Asia during 1979-2012
775 using the MEGAN scheme and taking into account both climate and land-use changes.
776 Their results showed widespread increases in the emissions over China but moderate
777 decreases in Indonesia. In contrast, the YIBs model with the MEGAN scheme simulates
778 widespread reductions in the same areas for 1980-2011 (Fig. 6c). The discrepancies
779 between studies are accounted for by differences in the drivers including land cover
780 change, meteorology, and CO₂ inhibition effects. The YIBs model is driven with land
781 cover data from Hurtt et al. (2011), which estimates an increase of crop (non-isoprene
782 emitter) fraction in East China by 0.32% per year in the last 3 decades, at the cost of the
783 coverage loss by 0.12% a⁻¹ for DBF and 0.14% a⁻¹ for ENF (strong BVOC emitters).
784 However, the data from Ramankutty and Foley (1999), used by Stavrakou et al. (2014)
785 with updates to 2007, show a reduction of the crop fraction over East China for the
786 similar period. In addition, the ERA-Interim PAR used in Stavrakou et al. (2014) shows
787 an increasing trend in southeast China (c.f. their Fig. 5c). On the contrary, the WFDEI
788 PAR for YIBs exhibits a declining trend in the same region (Fig. S1b), leading to a
789 reduction in isoprene emissions. The WFDEI surface solar radiation is based on the ERA-
790 Interim radiation but is adjusted using the average cloud cover from the Climatic
791 Research Unit (CRU) and taking into account the effects of interannual changes in
792 atmospheric aerosols (Weedon et al., 2011). Finally, the YIBs simulations include CO₂
793 inhibition effects on BVOC emissions, which were neglected in Stavrakou et al. (2014).

794
795 Naik et al. (2004) predicted a global trend of 1.3 Tg C a⁻² for isoprene emissions during
796 1971-1990 using the Integrated Biospheric Simulator (IBIS) driven with monthly mean
797 CRU meteorology. Lathiere et al. (2006) estimated an increasing global trend of 0.3 Tg C
798 a⁻² for 1983-1995 using the ORCHIDEE (Organizing Carbon and Hydrology in Dynamic
799 EcosystEms) vegetation model driven with sub-daily variables from the NCEP/DOE
800 (National Center for Environmental Predictions/Department of Energy) Reanalysis 2.
801 Muller et al. (2008) reported a global increase of 4.5 Tg C a⁻² for 1995-2006 using a

Xu Yue 10/6/15 1:41 PM
Moved (insertion) [1]

Xu Yue 10/6/15 1:41 PM
Moved (insertion) [2]

Xu Yue 10/6/15 1:41 PM
Moved (insertion) [3]

Xu Yue 10/6/15 1:41 PM
Moved (insertion) [4]

802 canopy environmental model and the NCEP meteorological data. In contrast to these
803 previous studies, YIBs with the MEGAN scheme simulates a decreasing trend of ~1 Tg C
804 a⁻² in the past 3 decades. The main cause of the discrepancy in the sign of change is the
805 missing CO₂ inhibition effects in the previous studies. In addition, differences in
806 vegetation models, meteorological forcings, and time frames of investigation also likely
807 contribute. The YIBs result is consistent with a recent study by Sindelarova et al. (2014),
808 who reported a decreasing trend of ~1.2 Tg C a⁻² for global isoprene emissions during
809 1980-2010 using the MEGAN scheme and inclusion of a CO₂ inhibition parameterization
810 from Heald et al. (2009).

812 4.3 Impacts of CO₂ effects

813
814 Similar to the multi-model ensemble predictions (Sitch et al., 2015), we found that global
815 trends in carbon fluxes are dominantly driven by CO₂ fertilization (Figs. 2 and 5). In the
816 YIBs, the global responses to elevated [CO₂] is 0.2% ppm⁻¹ for GPP and 0.27% ppm⁻¹ for
817 NPP, with relatively uniform spatial distribution (Figs. [S7a](#) and [S7b](#)). The GPP response
818 falls within the range of 0.05-0.21% ppm⁻¹ predicted by 10 terrestrial models (Piao et al.,
819 2013) and that of 0.01-0.32% ppm⁻¹ observed from multiple free-air CO₂ enrichment
820 (FACE) sites (Ainsworth and Long, 2005). The NPP response is higher than the model
821 ensemble of 0.16% ppm⁻¹ (Piao et al., 2013) and the observed median value of 0.13%
822 ppm⁻¹ (Norby et al., 2005), suggesting that CO₂ fertilization to NPP may be
823 overestimated in the YIBs. One possible cause is the omission of N limitation in the
824 model, which could reduce CO₂ responses by half (Piao et al., 2013). Elevated [CO₂]
825 leads to increases of 0.023 Pg C a⁻¹ ppm⁻¹ in NEP, within the multi-model range of 0.003-
826 0.06 Pg C a⁻¹ ppm⁻¹ (Piao et al., 2013).

827
828 Responses of BVOC emissions to elevated [CO₂] are different between PS_BVOC and
829 MEGAN schemes (Figs. [S7c](#) and [S7d](#)). PS_BVOC includes both CO₂ fertilization (on
830 photosynthesis) and inhibition (on isoprene) effects, leading to moderate but generally
831 positive changes in isoprene emissions. In contrast, emissions from the MEGAN scheme
832 are not dependent on foliar photosynthesis and as a result only CO₂ inhibition is enforced.

Xu Yue 10/6/15 1:41 PM
Moved (insertion) [5]

Unknown
Field Code Changed

Xu Yue 10/6/15 1:41 PM
Moved (insertion) [6]

Xu Yue 10/6/15 1:41 PM
Deleted: S10a

Xu Yue 10/6/15 1:41 PM
Deleted: S10b

Xu Yue 10/6/15 1:41 PM
Deleted: S10c

Xu Yue 10/6/15 1:41 PM
Deleted: S10d

837 Chamber experiments show contrary tendencies for photosynthesis and isoprene in
838 response to elevated [CO₂] (Possell et al., 2005), supporting the simulations with
839 MEGAN. In addition, the magnitude of CO₂ inhibition implemented in MEGAN (-0.25%
840 ppm⁻¹) is close to observations (-0.26% ppm⁻¹) in Possell et al. (2005). However, most of
841 these experiments are conducted for short-term period and cannot detect LAI changes due
842 to the long-term CO₂ fertilization. In addition, the impacts of CO₂ are dependent on
843 species and environmental conditions (ambient temperature and light availability). For
844 example, Buckley (2001) found almost no responses in isoprene emissions to the elevated
845 [CO₂] for oak trees. Furthermore, experiments with high temperature and/or light density
846 show increasing isoprene at elevated [CO₂] (Sun et al., 2013). These studies suggest that
847 the real responses of isoprene emissions to CO₂ under long-term climate change may not
848 be so linear as predicted in MEGAN scheme. More sensitivity experiments and long-term
849 samplings are required to identify CO₂-isoprene relationships on broad range of biomes
850 and locations.

851

852 | 4.4 Impacts of meteorology

853

854 Predicted long-term trends show large deviations against observations at tropical areas
855 (Fig. 3), where meteorology plays important and complex roles. Responses of carbon
856 | fluxes to temperature are more diverse than to CO₂ (Figs. S8a and S8b). In the YIBs,
857 negative responses of GPP and NPP are predicted in tropical areas, where soil moisture
858 availability limits plant functions (e.g. stomatal conductance) to the increased
859 temperature. Furthermore, for tropical rainforests where ambient temperature is higher
860 than optimal photosynthetic temperature (25-30°C), additional warming decreases carbon
861 assimilation, especially for NPP because of simultaneous increases in plant respiration
862 (Liang et al., 2013). On the contrary, warming leads to enhanced GPP and NPP at wetter
863 and cooler areas in the NH subtropics. Such spatial pattern is consistent with multi-model
864 ensemble predictions (Piao et al., 2013). On the global scale, warming results in changes
865 of -0.7% °C⁻¹ for GPP in YIBs, falling within the range of -1.6-1.4% °C⁻¹ estimated by 10
866 | models (Piao et al., 2013). Predicted NPP responses of -15-6% °C⁻¹ (Fig. S8b) is not so
867 positive as the measurements of -8-40% °C⁻¹, probably because most of current warming

Xu Yue 10/6/15 1:41 PM

Deleted: 3

Xu Yue 10/6/15 1:41 PM

Deleted: S11a

Xu Yue 10/6/15 1:41 PM

Deleted: S11b

Xu Yue 10/6/15 1:41 PM

Deleted: S11b

872 experiments are located in subtropics of NH (Wu et al., 2011). Elevated temperature
873 changes NEP by $-1.4 \text{ Pg C a}^{-1} \text{ } ^\circ\text{C}^{-1}$, also within the multi-model range of $-5\sim-1 \text{ Pg C a}^{-1}$
874 $^\circ\text{C}^{-1}$ (Piao et al., 2013). Simulated isoprene emissions with PS_BVOC show similar
875 warming responses as that of carbon fluxes (Fig. S8c), except for tropical rainforests
876 where the former is positive while the latter is negative. Such decoupling is attributed to
877 the differences in optimal temperatures between isoprene (35-40 $^\circ\text{C}$) and photosynthesis
878 (25-30 $^\circ\text{C}$). Simulations with MEGAN scheme show very strong temperature dependence
879 of 6-15% $^\circ\text{C}^{-1}$ (Fig. S8d), consistent with measurements of 5-20% $^\circ\text{C}^{-1}$ for aspen
880 (Niinemets and Sun, 2015) and 9-12% $^\circ\text{C}^{-1}$ for oak (Li et al., 2011). However,
881 experiments with some other species (e.g. spruce in Kivimaenpaa et al. (2013)) show no
882 responses or moderate ones, suggesting that warming sensitivity of isoprene emissions
883 might be dependent on species and ambient conditions.

884

885 Responses to PAR are mostly positive and distributed evenly, with global sensitivity of
886 $0.3\% \text{ W}^{-1} \text{ m}^2$ for GPP and $0.5\% \text{ W}^{-1} \text{ m}^2$ for NPP (Figs. S9a and S9b). Isoprene emissions
887 from both PS_BVOC and MEGAN schemes show similar responses to PAR, with larger
888 sensitivity in subtropics than that in tropics (Figs. S9c and S9d), likely because the
889 ambient PAR is higher at lower latitude, leading to slower responses of isoprene
890 emissions to the unit changes of light (Guenther et al., 1993). YIBs simulations show that
891 PAR is not the driver of long-term trends in carbon fluxes and BVOC emissions (Fig. 4),
892 likely because changes in solar radiation is limited in the past 3 decades (Figs. S1b).

893

894 Soil moisture dominates climate-driven flux changes in tropical areas (Fig. 4). In YIBs
895 model, changes in soil water availability affect carbon assimilation through the alteration
896 of leaf stomatal conductance and plant phenology (especially for shrublands and
897 grasslands in arid regions). Both GPP and NPP show strong responses to soil wetness
898 variations, especially over tropics where $>10\%$ changes are found for every increase of
899 0.01 in soil wetness at 1.5 m (Figs. S10a and S10b). On the global scale, GPP changes by
900 $4.7\% \text{ } 0.01^{-1}$ and NPP by $5.5\% \text{ } 0.01^{-1}$ in response to soil wetness. Although experiments
901 also show rapid reductions in carbon assimilation due to drought stress (e.g., Ruehr et al.,
902 2012; Xia et al., 2014), the magnitude of such influence is difficult to evaluate because

Xu Yue 10/6/15 1:41 PM

Deleted: S11c

Xu Yue 10/6/15 1:41 PM

Deleted: S11d

Xu Yue 10/6/15 1:41 PM

Deleted: S12a

Xu Yue 10/6/15 1:41 PM

Deleted: S12b

Xu Yue 10/6/15 1:41 PM

Deleted: S12c

Xu Yue 10/6/15 1:41 PM

Deleted: S12d

Xu Yue 10/6/15 1:41 PM

Deleted: S2b and S3b

Xu Yue 10/6/15 1:41 PM

Deleted: S13a

Xu Yue 10/6/15 1:41 PM

Deleted: S13b

912 different metrics and depths of soil water are used in measurements. Isoprene emissions
913 from PS_BVOC show similar soil-wetness responses to that of GPP (Fig. S10c),
914 indicating that drought reduces BVOC emissions. However, observations show
915 insignificant changes of isoprene with mild drought stress (e.g., Pegoraro et al., 2006),
916 though such drought tolerance is strongly weakened at severe drought and/or warm
917 conditions (Centritto et al., 2011). Consistent with these experiments, MEGAN scheme
918 does not include drought inhibition on isoprene emissions. Simulations with YIBs show
919 large responses of BVOC to soil wetness in tropical areas (Fig. S10d), mainly because of
920 the changes in drought-dependent phenology.

921

922 4.5 Impacts of land use change

923

924 Changes of land use show moderate impacts on global carbon budget (Fig. 2) and BVOC
925 emissions (Fig. 6) in the past 3 decades, though regional perturbations are found in China
926 and Europe. The afforestation in Europe helps promote regional carbon uptake, resulting
927 in more reasonable trends in LAI compared with remote sensing data (Fig. 1). However,
928 the expansion of crop in China leads to a reduction in LAI, which is not supported by the
929 satellite data. One possible cause is the uncertainty in crop fraction, because data from
930 Hurr et al. (2011), used by YIBs, show crop expansion while data from Ramankutty and
931 Foley (1999) suggest reductions of the crop fraction over East China over the similar
932 period. The role of land use change in our simulation might be conservative because we
933 consider only land cover changes. Perturbed emissions from land use management, such
934 as forest logging, cropping practice, use of fertilizer, fire management and so on
935 (Houghton, 2010) may alter regional carbon budget by changing carbon sinks to sources.
936 Studies including gross emissions of land use perturbation estimated a global net land
937 source to atmosphere, which shows decreasing trend in the last 3 decades (Ciais et al.,
938 2013). Such change may help strengthen net land carbon sink but is missing in our study.

939

940 4.6 Impacts of biospheric changes

941

Xu Yue 10/6/15 1:41 PM

Deleted: S13c

Xu Yue 10/6/15 1:41 PM

Deleted: S13d

Xu Yue 10/6/15 1:41 PM

Deleted: Different climatic forcings may lead to varied trends in the simulations of carbon fluxes (Figs. 2 and S1) and BVOC emissions (Figs. 6 and S4). Trends of meteorology show large discrepancies between WFDEI and MERRA data sets over tropical areas, especially in Amazon and central Africa (Figs. S2 and S3). Such uncertainty strongly affects the calculated global trends in carbon budget and also influences the identification of drivers for those changes. For example, with MERRA forcing, YIBs model simulates global increases of 239 Tg C a⁻² in NPP and 59 Tg C a⁻² in NEP over the past 3 decades (Table S1), both values are higher than that with WFDEI forcing (185 for NPP and 3 for NEP, Table 3) and much closer to the multi-model ensemble estimates (218 for NPP and 55 for NEP) as shown in Sitch et al. (2015). The stronger trends in carbon fluxes with MERRA are mainly attributed to the reductions in Amazonia temperature (Fig. S3a), which drives the large enhancement of regional GPP (Fig. 4b) and also overweighs the contribution of CO₂ fertilization (Fig. S1d). However, we are conservative about simulations with MERRA because the associated changes of meteorological fields are too strong in the tropics (Fig. S3). Our results show the large climate-driven uncertainties in the estimate of long-term trends in carbon fluxes, indicating the necessity of forcing inter-comparisons in addition to model inter-comparisons (e.g., Huntzinger et al., 2013; Piao et al., 2013) [11]

Xu Yue 10/6/15 1:41 PM

Deleted: 4

Xu Yue 10/6/15 1:41 PM

Deleted: 5

981 The land biosphere has experienced significant changes in the past 3 decades. At north of
982 30°N, changes in LAI account for 25% of the trends in regional carbon fluxes and
983 isoprene emissions. However, the extension of growing season alone makes insignificant
984 contributions to the increased carbon assimilation. This conclusion is inconsistent with
985 site-level observations that show evident increases in carbon assimilation at early spring
986 and/or late autumn in recent decades (Dragoni et al., 2011; Keenan et al., 2014). The
987 causes for such discrepancies lie in two. First, phenology at specific location may exhibit
988 much more intense changes than that at larger scale. For example, Dragoni et al. (2011)
989 estimated extensions of growing season by 2.3-3.3 day a⁻¹ in Morgan-Monroe State
990 Forest in south-central Indiana of US for 1998-2008. The magnitude of this change is ~10
991 times larger than the observed value of 0.36 day a⁻¹ from satellite and simulated value of
992 0.22 day a⁻¹ with YIBs for the northern lands. Second, enhanced temperature also
993 contributes to the stronger uptake at early spring and late autumn. One difficulty for the
994 observation-based estimate of phenological impacts is that extension of growing season is
995 accompanied by warmer climate, which may stimulate both carbon assimilation and
996 BVOC production. In a recent study, Barlow et al. (2015) found invariant length of land
997 carbon uptake period at high northern latitudes based on the first time differential of
998 atmospheric CO₂ concentrations, suggesting that increased greenness is not necessarily
999 equal to enhanced carbon uptake in shoulder seasons. Furthermore, Barlow et al. (2015)
1000 showed that enhanced peak uptake is the main driver for the strengthened carbon sink at
1001 high northern latitudes over the past 4 decades. These conclusions are supportive of our
1002 simulations for the monthly trends at subtropical regions (North America, Europe, and
1003 East Asia) (Fig. S5).

1004
1005

1006 **5 Conclusions**

1007

1008 With YIBs model, we estimated global increases of carbon assimilation especially at
1009 tropical areas for 1982-2011. This trend is mainly attributed to the widespread CO₂
1010 fertilization effect, and jointly affected by changes in meteorology and land cover.
1011 Increase of temperature promotes carbon uptake of forest ecosystems at high latitudes

Xu Yue 10/6/15 1:41 PM

Deleted: S8).

1013 (>30°N) while drought tendency dampens GPP and NPP of grasslands and shrublands at
1014 low latitudes (30°S-30°N). The widespread increases of LAI at northern lands account for
1015 ~25% of the regional GPP trends. Significant changes in phenology are found at north of
1016 30°N; however, this temperature-driven phenological change alone is not promoting
1017 regional carbon assimilation. Changes in land use show limited influences on global
1018 carbon fluxes, except for some regional impacts over Europe (afforestation) and China
1019 (deforestation). Due to the simultaneous enhancement in soil respiration, land carbon sink
1020 has remained almost stable in the past 3 decades. The YIBs model does not yet include a
1021 fully coupled carbon-nitrogen cycle, thus the model may overestimate CO₂ fertilization
1022 effects. On the contrary, implementation of drought-dependent phenology may amplify
1023 drought inhibition effects on photosynthesis and result in an underestimation of carbon
1024 uptake.

1025

1026 We estimated global trends of BVOC emissions with two schemes. Simulations with
1027 PS_BVOC scheme show increasing isoprene emissions, mainly attributed to the increases
1028 of temperature. For this scheme, CO₂ effects are neutralized due to both fertilization (on
1029 photosynthesis) and inhibition (on isoprene). Simulations with MEGAN scheme show
1030 decreasing emissions of isoprene and monoterpene because of CO₂ inhibition, especially
1031 in the tropics. In subtropical areas, both schemes predict regional increases of BVOC
1032 emissions in Europe following the warming trend and afforestation, but reductions in the
1033 U.S. and China due to cropland expansion.

1034

1035

1036 *Acknowledgements.* Funding support for this research is provided by the NASA
1037 Atmospheric Composition Campaign Data Analysis and Modeling Program. This project
1038 was supported in part by the facilities and staff of the Yale University Faculty of Arts and
1039 Sciences High Performance Computing Center.

1040

1041

Xu Yue 10/6/15 1:41 PM

Deleted: In contrast, using alternate meteorological forcings, we found enhancement of land carbon sink due to increasing uptake in Amazon.

1046 **References**

- 1047 Ainsworth, E. A., and Long, S. P.: What have we learned from 15 years of free-air CO₂
1048 enrichment (FACE)? A meta-analytic review of the responses of photosynthesis,
1049 canopy, *New Phytol*, 165, 351-371, doi:10.1111/J.1469-8137.2004.01224.X, 2005.
- 1050 Arneth, A., Niinemets, U., Pressley, S., Back, J., Hari, P., Karl, T., Noe, S., Prentice, I.
1051 C., Serca, D., Hickler, T., Wolf, A., and Smith, B.: Process-based estimates of
1052 terrestrial ecosystem isoprene emissions: incorporating the effects of a direct CO₂-
1053 isoprene interaction, *Atmos Chem Phys*, 7, 31-53, doi:10.5194/acp-7-31-2007, 2007.
- 1054 Barlow, J. M., Palmer, P. I., Bruhwiler, L. M., and and Tans, P.: Analysis of CO₂ mole
1055 fraction data: first evidence of large-scale changes in CO₂ uptake at high northern
1056 latitudes, *Atmos. Chem. Phys. Discuss.*, 15, 7089-7139, doi:10.5194/acpd-15-7089-
1057 2015, 2015.
- 1058 Beer, C., Reichstein, M., Tomelleri, E., Ciais, P., Jung, M., Carvalhais, N., Rodenbeck,
1059 C., Arain, M. A., Baldocchi, D., Bonan, G. B., Bondeau, A., Cescatti, A., Lasslop, G.,
1060 Lindroth, A., Lomas, M., Luyssaert, S., Margolis, H., Oleson, K. W., Rouspard, O.,
1061 Veenendaal, E., Viovy, N., Williams, C., Woodward, F. I., and Papale, D.: Terrestrial
1062 Gross Carbon Dioxide Uptake: Global Distribution and Covariation with Climate,
1063 *Science*, 329, 834-838, doi:10.1126/Science.1184984, 2010.
- 1064 Buckley, P. T.: Isoprene emissions from a Florida scrub oak species grown in ambient
1065 and elevated carbon dioxide, *Atmos Environ*, 35, 631-634, doi:10.1016/S1352-
1066 2310(00)00332-0, 2001.
- 1067 Buitenwerf, R., Rose, L., and Higgins, S. I.: Three decades of multi-dimensional change
1068 in global leaf phenology, *Nat Clim Change*, 5, 364-368, 2015.
- 1069 Carslaw, K. S., Boucher, O., Spracklen, D. V., Mann, G. W., Rae, J. G. L., Woodward,
1070 S., and Kulmala, M.: A review of natural aerosol interactions and feedbacks within
1071 the Earth system, *Atmos. Chem. Phys.*, 10, 1701-1737, doi:10.5194/acp-10-1701-
1072 2010, 2010.
- 1073 Centritto, M., Brilli, F., Fodale, R., and Loreto, F.: Different sensitivity of isoprene
1074 emission, respiration and photosynthesis to high growth temperature coupled with
1075 drought stress in black poplar (*Populus nigra*) saplings, *Tree Physiol*, 31, 275-286,
1076 doi:10.1093/Treephys/Tpql12, 2011.
- 1077 Ciais, P., Sabine, C., Bala, G., Bopp, L., Brovkin, V., Canadell, J., Chhabra, A., DeFries,
1078 R., Galloway, J., Heimann, M., Jones, C., Le Quere, C., Myneni, R., Piao, S., and
1079 Thornton, P.: Carbon and other biogeochemical cycles, in: *Climate Change 2013: The
1080 Physical Science Basis. Contribution of Working Group I to the Fifth Assessment
1081 Report of the Intergovernmental Panel on Climate Change*, edited by: Stocker, T. F.,
1082 Qin, D., Plattner, G.-K., Tignor, M., Allen, S. K., Boschung, J., Nauels, A., Xia, Y.,
1083 Bex, V., and Midgley, P. M., Cambridge University Press, Cambridge, United
1084 Kingdom and New York, NY, USA, 465-570, 2013.
- 1085 Collatz, G. J., Ball, J. T., Grivet, C., and Berry, J. A.: Physiological and Environmental-
1086 Regulation of Stomatal Conductance, Photosynthesis and Transpiration - a Model
1087 That Includes a Laminar Boundary-Layer, *Agr Forest Meteorol*, 54, 107-136,
1088 doi:10.1016/0168-1923(91)90002-8, 1991.
- 1089 Cox, P. M.: Description of the "TRIFFID" Dynamic Global Vegetation Model, Hadley
1090 Centre technical note 24, [Berks, UK](#), 2001.

- 1091 Defries, R. S., Hansen, M. C., Townshend, J. R. G., Janetos, A. C., and Loveland, T. R.:
 1092 A new global 1-km dataset of percentage tree cover derived from remote sensing,
 1093 *Global Change Biol*, 6, 247-254, doi:10.1046/J.1365-2486.2000.00296.X, 2000.
- 1094 Dragoni, D., Schmid, H. P., Wayson, C. A., Potter, H., Grimmond, C. S. B., and
 1095 Randolph, J. C.: Evidence of increased net ecosystem productivity associated with a
 1096 longer vegetated season in a deciduous forest in south-central Indiana, USA, *Global*
 1097 *Change Biol*, 17, 886-897, doi:10.1111/J.1365-2486.2010.02281.X, 2011.
- 1098 Farquhar, G. D., Caemmerer, S. V., and Berry, J. A.: A Biochemical-Model of
 1099 Photosynthetic Co₂ Assimilation in Leaves of C-3 Species, *Planta*, 149, 78-90,
 1100 doi:10.1007/Bf00386231, 1980.
- 1101 Guenther, A. B., Zimmerman, P. R., Harley, P. C., Monson, R. K., and Fall, R.: Isoprene
 1102 and Monoterpene Emission Rate Variability - Model Evaluations and Sensitivity
 1103 Analyses, *J. Geophys. Res.*, 98, 12609-12617, doi:10.1029/93jd00527, 1993.
- 1104 Guenther, A. B., Hewitt, C. N., Erickson, D., Fall, R., Geron, C., Graedel, T., Harley, P.,
 1105 Klinger, L., Lerdau, M., McKay, W. A., Pierce, T., Scholes, B., Steinbrecher, R.,
 1106 Tallamraju, R., Taylor, J., and Zimmerman, P.: A Global-Model of Natural Volatile
 1107 Organic-Compound Emissions, *J. Geophys. Res.*, 100, 8873-8892,
 1108 doi:10.1029/94jd02950, 1995.
- 1109 Hansen, M. C., DeFries, R. S., Townshend, J. R. G., Carroll, M., Dimiceli, C., and
 1110 Sohlberg, R. A.: Global Percent Tree Cover at a Spatial Resolution of 500 Meters:
 1111 First Results of the MODIS Vegetation Continuous Fields Algorithm, *Earth Interact*,
 1112 7, 2003.
- 1113 Heald, C. L., Wilkinson, M. J., Monson, R. K., Alo, C. A., Wang, G. L., and Guenther,
 1114 A.: Response of isoprene emission to ambient CO₂ changes and implications for
 1115 global budgets, *Global Change Biol*, 15, 1127-1140, doi:10.1111/J.1365-
 1116 2486.2008.01802.X, 2009.
- 1117 Heinsch, F. A., Zhao, M. S., Running, S. W., Kimball, J. S., Nemani, R. R., Davis, K. J.,
 1118 Bolstad, P. V., Cook, B. D., Desai, A. R., Ricciuto, D. M., Law, B. E., Oechel, W. C.,
 1119 Kwon, H., Luo, H. Y., Wofsy, S. C., Dunn, A. L., Munger, J. W., Baldocchi, D. D.,
 1120 Xu, L. K., Hollinger, D. Y., Richardson, A. D., Stoy, P. C., Siqueira, M. B. S.,
 1121 Monson, R. K., Burns, S. P., and Flanagan, L. B.: Evaluation of remote sensing based
 1122 terrestrial productivity from MODIS using regional tower eddy flux network
 1123 observations, *Ieee T Geosci Remote*, 44, 1908-1925, doi:10.1109/Tgrs.2005.853936,
 1124 2006.
- 1125 Houghton, R. A.: How well do we know the flux of CO₂ from land-use change?, *Tellus*
 1126 B, 62, 337-351, doi:Doi 10.1111/J.1600-0889.2010.00473.X, 2010.
- 1127 | Hurtt, G. C., Chini, L. P., Frolking, S., Betts, R. A., Feddema, J., Fischer, G., Fisk, J. P.,
 1128 Hibbard, K., Houghton, R. A., Janetos, A., Jones, C. D., Kindermann, G., Kinoshita,
 1129 T., Goldewijk, K. K., Riahi, K., Shevliakova, E., Smith, S., Stehfest, E., Thomson, A.,
 1130 Thornton, P., van Vuuren, D. P., and Wang, Y. P.: Harmonization of land-use
 1131 scenarios for the period 1500-2100: 600 years of global gridded annual land-use
 1132 transitions, wood harvest, and resulting secondary lands, *Climatic Change*, 109, 117-
 1133 161, doi:10.1007/S10584-011-0153-2, 2011.
- 1134 Jeong, S. J., Ho, C. H., Gim, H. J., and Brown, M. E.: Phenology shifts at start vs. end of
 1135 growing season in temperate vegetation over the Northern Hemisphere for the period

Xu Yue 10/6/15 1:41 PM

Deleted: Huntzinger, D. N., Schwalm, C., Michalak, A. M., Schaefer, K., King, A. W., Wei, Y., Jacobson, A., Liu, S., Cook, R. B., Post, W. M., Berthier, G., Hayes, D., Huang, M., Ito, A., Lei, H., Lu, C., Mao, J., Peng, C. H., Peng, S., Poulter, B., Ricciuto, D., Shi, X., Tian, H., Wang, W., Zeng, N., Zhao, F., and Zhu, Q.: The North American Carbon Program Multi-Scale Synthesis and Terrestrial Model Intercomparison Project - Part 1: Overview and experimental design, *Geosci Model Dev*, 6, 2121-2133, doi:10.5194/Gmd-6-2121-2013, 2013.

1149 1982-2008, *Global Change Biol*, 17, 2385-2399, doi:10.1111/J.1365-
1150 2486.2011.02397.X, 2011.

1151 Jung, M., Reichstein, M., and Bondeau, A.: Towards global empirical upscaling of
1152 FLUXNET eddy covariance observations: validation of a model tree ensemble
1153 approach using a biosphere model, *Biogeosciences*, 6, 2001-2013, doi:10.5194/bg-6-
1154 2001-2009, 2009.

1155 Keenan, T. F., Gray, J., Friedl, M. A., Toomey, M., Bohrer, G., Hollinger, D. Y.,
1156 Munger, J. W., O'Keefe, J., Schmid, H. P., SueWing, I., Yang, B., and Richardson, A.
1157 D.: Net carbon uptake has increased through warming-induced changes in temperate
1158 forest phenology, *Nat Clim Change*, 4, 598-604, doi:10.1038/Nclimate2253, 2014.

1159 Kivimaenpaa, M., Riikonen, J., Ahonen, V., Tervahauta, A., and Holopainen, T.:
1160 Sensitivity of Norway spruce physiology and terpenoid emission dynamics to
1161 elevated ozone and elevated temperature under open-field exposure, *Environ Exp*
1162 *Bot*, 90, 32-42, doi:10.1016/J.Envexpbot.2012.1t004, 2013.

1163 Lathiere, J., Hauglustaine, D. A., Friend, A. D., De Noblet-Ducoudre, N., Viovy, N., and
1164 Folberth, G. A.: Impact of climate variability and land use changes on global biogenic
1165 volatile organic compound emissions, *Atmos Chem Phys*, 6, 2129-2146,
1166 doi:10.5194/acp-6-2129-2006, 2006.

1167 Le Quere, C., Raupach, M. R., Canadell, J. G., Marland, G., Bopp, L., Ciais, P., Conway,
1168 T. J., Doney, S. C., Feely, R. A., Foster, P., Friedlingstein, P., Gurney, K., Houghton,
1169 R. A., House, J. I., Huntingford, C., Levy, P. E., Lomas, M. R., Majkut, J., Metzl, N.,
1170 Ometto, J. P., Peters, G. P., Prentice, I. C., Randerson, J. T., Running, S. W.,
1171 Sarmiento, J. L., Schuster, U., Sitch, S., Takahashi, T., Viovy, N., van der Werf, G.
1172 R., and Woodward, F. I.: Trends in the sources and sinks of carbon dioxide, *Nat*
1173 *Geosci*, 2, 831-836, doi:10.1038/Ngeo689, 2009.

1174 Li, Z. R., Ratliff, E. A., and Sharkey, T. D.: Effect of Temperature on Postillumination
1175 Isoprene Emission in Oak and Poplar, *Plant Physiol*, 155, 1037-1046,
1176 doi:10.1104/Pp.110.167551, 2011.

1177 Liang, J. Y., Xia, J. Y., Liu, L. L., and Wan, S. Q.: Global patterns of the responses of
1178 leaf-level photosynthesis and respiration in terrestrial plants to experimental warming,
1179 *J Plant Ecol*, 6, 437-447, doi:10.1093/Jpe/Rtt003, 2013.

1180 Mao, J. F., Shi, X. Y., Thornton, P. E., Hoffman, F. M., Zhu, Z. C., and Myneni, R. B.:
1181 Global Latitudinal-Asymmetric Vegetation Growth Trends and Their Driving
1182 Mechanisms: 1982-2009, *Remote Sens*, 5, 1484-1497, doi:Doi 10.3390/Rs5031484,
1183 2013.

1184 Marais, E. A., Jacob, D. J., Kurosu, T. P., Chance, K., Murphy, J. G., Reeves, C., Mills,
1185 G., Casadio, S., Millet, D. B., Barkley, M. P., Paulot, F., and Mao, J.: Isoprene
1186 emissions in Africa inferred from OMI observations of formaldehyde columns,
1187 *Atmos Chem Phys*, 12, 6219-6235, doi:10.5194/Acp-12-6219-2012, 2012.

1188 Meinshausen, M., Smith, S. J., Calvin, K., Daniel, J. S., Kainuma, M. L. T., Lamarque, J.
1189 F., Matsumoto, K., Montzka, S. A., Raper, S. C. B., Riahi, K., Thomson, A., Velders,
1190 G. J. M., and van Vuuren, D. P. P.: The RCP greenhouse gas concentrations and their
1191 extensions from 1765 to 2300, *Climatic Change*, 109, 213-241, doi:10.1007/S10584-
1192 011-0156-Z, 2011.

1193 Monson, R. K., Trahan, N., Rosenstiel, T. N., Veres, P., Moore, D., Wilkinson, M.,
1194 Norby, R. J., Volder, A., Tjoelker, M. G., Briske, D. D., Karnosky, D. F., and Fall,

1195 R.: Isoprene emission from terrestrial ecosystems in response to global change:
 1196 minding the gap between models and observations, *Philos T R Soc A*, 365, 1677-
 1197 1695, doi:10.1098/Rsta.2007.2038, 2007.

1198 Muller, J. F., Stavrakou, T., Wallens, S., De Smedt, I., Van Roozendael, M., Potosnak,
 1199 M. J., Rinne, J., Munger, B., Goldstein, A., and Guenther, A. B.: Global isoprene
 1200 emissions estimated using MEGAN, ECMWF analyses and a detailed canopy
 1201 environment model, *Atmos Chem Phys*, 8, 1329-1341, 2008.

1202 Naik, V., Delire, C., and Wuebbles, D. J.: Sensitivity of global biogenic isoprenoid
 1203 emissions to climate variability and atmospheric CO₂, *J. Geophys. Res.*, 109,
 1204 D06301, doi:10.1029/2003jd004236, 2004.

1205 Niinemets, U., and Sun, Z. H.: How light, temperature, and measurement and growth
 1206 [CO₂] interactively control isoprene emission in hybrid aspen, *J Exp Bot*, 66, 841-
 1207 851, doi:10.1093/Jxb/Eru443, 2015.

1208 Norby, R. J., DeLucia, E. H., Gielen, B., Calfapietra, C., Giardina, C. P., King, J. S.,
 1209 Ledford, J., McCarthy, H. R., Moore, D. J. P., Ceulemans, R., De Angelis, P., Finzi,
 1210 A. C., Karnosky, D. F., Kubiske, M. E., Lukac, M., Pregitzer, K. S., Scarascia-
 1211 Mugnozza, G. E., Schlesinger, W. H., and Oren, R.: Forest response to elevated CO₂
 1212 is conserved across a broad range of productivity, *P Natl Acad Sci USA*, 102, 18052-
 1213 18056, doi:10.1073/Pnas.0509478102, 2005.

1214 Oleson, K. W., Lawrence, D. M., Bonan, G. B., Drewniak, B., Huang, M., Koven, C. D.,
 1215 Levis, S., Li, F., Riley, W. J., Subin, Z. M., Swenson, S. C., Thornton, P. E.,
 1216 Bozbiyik, A., Fisher, R., Heald, C. L., Kluzek, E., Lamarque, J.-F., Lawrence, P. J.,
 1217 Leung, L. R., Lipscomb, W., Muszala, S., Ricciuto, D. M., Sacks, W., Sun, Y., Tang,
 1218 J., and Yang, Z.-L.: Technical Description of version 4.5 of the Community Land
 1219 Model (CLM), National Center for Atmospheric Research, Boulder, CONCAR
 1220 Technical Note NCAR/TN-478+STR, 434, 2013.

1221 Palmer, P. I., Abbot, D. S., Fu, T. M., Jacob, D. J., Chance, K., Kurosu, T. P., Guenther,
 1222 A., Wiedinmyer, C., Stanton, J. C., Pilling, M. J., Pressley, S. N., Lamb, B., and
 1223 Sumner, A. L.: Quantifying the seasonal and interannual variability of North
 1224 American isoprene emissions using satellite observations of the formaldehyde
 1225 column, *J Geophys Res-Atmos*, 111, D12315, doi:10.1029/2005jd006689, 2006.

1226 Pan, Y. D., Birdsey, R. A., Fang, J. Y., Houghton, R., Kauppi, P. E., Kurz, W. A.,
 1227 Phillips, O. L., Shvidenko, A., Lewis, S. L., Canadell, J. G., Ciais, P., Jackson, R. B.,
 1228 Pacala, S. W., McGuire, A. D., Piao, S. L., Rautiainen, A., Sitch, S., and Hayes, D.: A
 1229 Large and Persistent Carbon Sink in the World's Forests, *Science*, 333, 988-993,
 1230 doi:10.1126/Science.1201609, 2011.

1231 Pegoraro, E., Rey, A., Abrell, L., Vanharen, J., and Lin, G. H.: Drought effect on
 1232 isoprene production and consumption in Biosphere 2 tropical rainforest, *Global
 1233 Change Biol*, 12, 456-469, doi:Doi 10.1111/J.1365-2486.2006.01112.X, 2006.

1234 Piao, S. L., Friedlingstein, P., Ciais, P., Viovy, N., and Demarty, J.: Growing season
 1235 extension and its impact on terrestrial carbon cycle in the Northern Hemisphere over
 1236 the past 2 decades, *Global Biogeochem Cy*, 21, Gb3018, doi:10.1029/2006gb002888,
 1237 2007.

1238 Piao, S. L., Sitch, S., Ciais, P., Friedlingstein, P., Peylin, P., Wang, X. H., Ahlstrom, A.,
 1239 Anav, A., Canadell, J. G., Cong, N., Huntingford, C., Jung, M., Levis, S., Levy, P. E.,
 1240 Li, J. S., Lin, X., Lomas, M. R., Lu, M., Luo, Y. Q., Ma, Y. C., Myneni, R. B.,

- 1241 Poulter, B., Sun, Z. Z., Wang, T., Viovy, N., Zaehle, S., and Zeng, N.: Evaluation of
 1242 terrestrial carbon cycle models for their response to climate variability and to CO₂
 1243 trends, *Global Change Biol*, 19, 2117-2132, doi:10.1111/Gcb.12187, 2013.
- 1244 Possell, M., Hewitt, C. N., and Beerling, D. J.: The effects of glacial atmospheric CO₂
 1245 concentrations and climate on isoprene emissions by vascular plants, *Global Change*
 1246 *Biol*, 11, 60-69, doi:10.1111/J.1365-2486.2004.00889.X, 2005.
- 1247 | Ramankutty, N., and Foley, J. A.: Estimating historical changes in global land cover:
 1248 Croplands from 1700 to 1992, *Global Biogeochem Cy*, 13, 997-1027,
 1249 doi:10.1029/1999gb900046, 1999.
- 1250 | Richardson, A. D., Hollinger, D. Y., Dail, D. B., Lee, J. T., Munger, J. W., and O'Keefe,
 1251 J.: Influence of spring phenology on seasonal and annual carbon balance in two
 1252 contrasting New England forests, *Tree Physiol*, 29, 321-331, doi:Doi
 1253 10.1093/Treephys/Tpn040, 2009.
- 1254 Richardson, A. D., Keenan, T. F., Migliavacca, M., Ryu, Y., Sonnentag, O., and Toomey,
 1255 M.: Climate change, phenology, and phenological control of vegetation feedbacks to
 1256 the climate system, *Agr Forest Meteorol*, 169, 156-173, 2013.
- 1257 | Ruehr, N. K., Martin, J. G., and Law, B. E.: Effects of water availability on carbon and
 1258 water exchange in a young ponderosa pine forest: Above- and belowground
 1259 responses, *Agr Forest Meteorol*, 164, 136-148, doi:10.1016/J.Agrformet.2012.05.015,
 1260 2012.
- 1261 Sarmiento, J. L., Gloor, M., Gruber, N., Beaulieu, C., Jacobson, A. R., Fletcher, S. E. M.,
 1262 Pacala, S., and Rodgers, K.: Trends and regional distributions of land and ocean
 1263 carbon sinks, *Biogeosciences*, 7, 2351-2367, doi:10.5194/Bg-7-2351-2010, 2010.
- 1264 Schaefer, K., Collatz, G. J., Tans, P., Denning, A. S., Baker, I., Berry, J., Prihodko, L.,
 1265 Suits, N., and Philpott, A.: Combined Simple Biosphere/Carnegie-Ames-Stanford
 1266 Approach terrestrial carbon cycle model, *J. Geophys. Res.*, 113, G03034,
 1267 doi:10.1029/2007jg000603, 2008.
- 1268 Scott, C. E., Rap, A., Spracklen, D. V., Forster, P. M., Carslaw, K. S., Mann, G. W.,
 1269 Pringle, K. J., Kivekas, N., Kulmala, M., Lihavainen, H., and Tunved, P.: The direct
 1270 and indirect radiative effects of biogenic secondary organic aerosol, *Atmos Chem*
 1271 *Phys*, 14, 447-470, doi:10.5194/Acp-14-447-2014, 2014.
- 1272 Sindelarova, K., Granier, C., Bouarar, I., Guenther, A., Tilmel, S., Stavrakou, T., Muller,
 1273 J. F., Kuhn, U., Stefani, P., and Knorr, W.: Global data set of biogenic VOC
 1274 emissions calculated by the MEGAN model over the last 30 years, *Atmos Chem*
 1275 *Phys*, 14, 9317-9341, doi:10.5194/Acp-14-9317-2014, 2014.
- 1276 Sitch, S., Friedlingstein, P., Gruber, N., Jones, S. D., Murray-Tortarolo, G., Ahlström, A.,
 1277 Doney, S. C., Graven, H., Heinze, C., Huntingford, C., Levis, S., Levy, P. E., Lomas,
 1278 M., Poulter, B., Viovy, N., Zaehle, S., Zeng, N., Arneth, A., Bonan, G., Bopp, L.,
 1279 Canadell, J. G., Chevallier, F., Ciais, P., Ellis, R., Gloor, M., Peylin, P., Piao, S. L.,
 1280 Quéré, C. L., Smith, B., Zhu, Z., and Myneni, R.: Recent trends and drivers of
 1281 regional sources and sinks of carbon dioxide, *Biogeosciences*, 12, 653-679, 2015.
- 1282 Stavrakou, T., Muller, J. F., Bauwens, M., De Smedt, I., Van Roozendaal, M., Guenther,
 1283 A., Wild, M., and Xia, X.: Isoprene emissions over Asia 1979-2012: impact of
 1284 climate and land-use changes, *Atmos Chem Phys*, 14, 4587-4605, doi:10.5194/Acp-
 1285 14-4587-2014, 2014.

Xu Yue 10/6/15 1:41 PM

Deleted: Poulter, B., Frank, D. C., Hodson, E. L., and Zimmermann, N. E.: Impacts of land cover and climate data selection on understanding terrestrial carbon dynamics and the CO₂ airborne fraction, *Biogeosciences*, 8, 2027-2036, doi:10.5194/Bg-8-2027-2011, 2011. .

Xu Yue 10/6/15 1:41 PM

Deleted: Reichle, R. H., Koster, R. D., De Lannoy, G. J. M., Forman, B. A., Liu, Q., Mahanama, S. P. P., and Toure, A.: Assessment and Enhancement of MERRA Land Surface Hydrology Estimates, *J Climate*, 24, 6322-6338, doi:10.1175/Jcli-D-10-05033.1, 2011. .

Xu Yue 10/6/15 1:41 PM

Deleted: Rienecker, M. M., Suarez, M. J., Gelaro, R., Todling, R., Bacmeister, J., Liu, E., Bosilovich, M. G., Schubert, S. D., Takacs, L., Kim, G. K., Bloom, S., Chen, J. Y., Collins, D., Conaty, A., Da Silva, A., Gu, W., Joiner, J., Koster, R. D., Lucchesi, R., Molod, A., Owens, T., Pawson, S., Pegion, P., Redder, C. R., Reichle, R., Robertson, F. R., Ruddick, A. G., Sienkiewicz, M., and Woollen, J.: MERRA: NASA's Modern-Era Retrospective Analysis for Research and Applications, *J Climate*, 24, 3624-3648, doi:10.1175/Jcli-D-11-00015.1, 2011. .

1313 Sun, Z. H., Hve, K., Vislap, V., and Niinemets, U.: Elevated [CO₂] magnifies isoprene
 1314 emissions under heat and improves thermal resistance in hybrid aspen, *J Exp Bot*, 64,
 1315 5509-5523, doi:10.1093/Jxb/Ert318, 2013.

1316 Unger, N., Harper, K., Zheng, Y., Kiang, N. Y., Aleinov, I., Arneth, A., Schurgers, G.,
 1317 Amelynck, C., Goldstein, A., Guenther, A., Heinesch, B., Hewitt, C. N., Karl, T.,
 1318 Laffineur, Q., Langford, B., McKinney, K. A., Misztal, P., Potosnak, M., Rinne, J.,
 1319 Pressley, S., Schoon, N., and Serça, D.: Photosynthesis-dependent isoprene emission
 1320 from leaf to planet in a global carbon–chemistry–climate model, *Atmos. Chem. Phys.*,
 1321 13, 17717-17791, doi:10.5194/acp-13-10243-2013, 2013.

1322 Unger, N.: On the role of plant volatiles in anthropogenic global climate change,
 1323 *Geophys Res Lett*, 41, 8563-8569, doi:10.1002/2014gl061616, 2014.

1324 Uppala, S. M., Kallberg, P. W., Simmons, A. J., Andrae, U., Bechtold, V. D., Fiorino,
 1325 M., Gibson, J. K., Haseler, J., Hernandez, A., Kelly, G. A., Li, X., Onogi, K.,
 1326 Saarinen, S., Sokka, N., Allan, R. P., Andersson, E., Arpe, K., Balmaseda, M. A.,
 1327 Beljaars, A. C. M., Van De Berg, L., Bidlot, J., Bormann, N., Caires, S., Chevallier,
 1328 F., Dethof, A., Dragosavac, M., Fisher, M., Fuentes, M., Hagemann, S., Holm, E.,
 1329 Hoskins, B. J., Isaksen, L., Janssen, P. A. E. M., Jenne, R., McNally, A. P., Mahfouf,
 1330 J. F., Morcrette, J. J., Rayner, N. A., Saunders, R. W., Simon, P., Sterl, A., Trenberth,
 1331 K. E., Untch, A., Vasiljevic, D., Viterbo, P., and Woollen, J.: The ERA-40 re-
 1332 analysis, *Q J Roy Meteor Soc*, 131, 2961-3012, doi:10.1256/Qj.04.176, 2005.

1333 von Caemmerer, S., and Farquhar, G. D.: Some Relationships between the Biochemistry
 1334 of Photosynthesis and the Gas-Exchange of Leaves, *Planta*, 153, 376-387, 1981.

1335 Weedon, G. P., Gomes, S., Viterbo, P., Shuttleworth, W. J., Blyth, E., Osterle, H., Adam,
 1336 J. C., Bellouin, N., Boucher, O., and Best, M.: Creation of the WATCH Forcing Data
 1337 and Its Use to Assess Global and Regional Reference Crop Evaporation over Land
 1338 during the Twentieth Century, *J Hydrometeorol*, 12, 823-848,
 1339 doi:10.1175/2011jhm1369.1, 2011.

1340 Weedon, G. P., Balsamo, G., Bellouin, N., Gomes, S., Best, M. J., and Viterbo, P.: The
 1341 WFDEI meteorological forcing data set: WATCH Forcing Data methodology applied
 1342 to ERA-Interim reanalysis data, *Water Resources Research*, 2014.

1343 Wofsy, S. C., Goulden, M. L., Munger, J. W., Fan, S. M., Bakwin, P. S., Daube, B. C.,
 1344 Bassow, S. L., and Bazzaz, F. A.: Net Exchange of Co₂ in a Midlatitude Forest,
 1345 *Science*, 260, 1314-1317, doi:10.1126/Science.260.5112.1314, 1993.

1346 Wu, Z. T., Dijkstra, P., Koch, G. W., Penuelas, J., and Hungate, B. A.: Responses of
 1347 terrestrial ecosystems to temperature and precipitation change: a meta-analysis of
 1348 experimental manipulation, *Global Change Biol*, 17, 927-942, doi:10.1111/J.1365-
 1349 2486.2010.02302.X, 2011.

1350 Xia, J. B., Zhang, G. C., Wang, R. R., and Zhang, S. Y.: Effect of soil water availability
 1351 on photosynthesis in *Ziziphus jujuba* var. *spinosus* in a sand habitat formed from
 1352 seashells: Comparison of four models, *Photosynthetica*, 52, 253-261, doi:Doi
 1353 10.1007/S11099-014-0030-0, 2014.

1354 Yue, X., and Unger, N.: Ozone vegetation damage effects on gross primary productivity
 1355 in the United States, *Atmos. Chem. Phys.*, 14, 9137-9153, doi:10.5194/acp-14-9137-
 1356 2014, 2014.

1357 | Yue, X., and Unger, N.: The Yale Interactive terrestrial Biosphere ~~model~~: description,
1358 | evaluation and implementation into NASA GISS ModelE2, Geosci. Model Dev., ~~8~~,
1359 | ~~2399-2417~~, doi:10.5194/gmd-8-2399-2015, 2015.

1360 | Yue, X., Unger, N., Keenan, T. F., Zhang, X., and Vogel, C. S.: Probing the past 30-year
1361 | phenology trend of U.S. deciduous forests, Biogeosciences, ~~12~~, ~~4693-4709~~,
1362 | doi:10.5194/~~bg-12-4693-2015~~, 2015.

1363 | Zhao, M. S., Heinsch, F. A., Nemani, R. R., and Running, S. W.: Improvements of the
1364 | MODIS terrestrial gross and net primary production global data set, Remote Sens
1365 | Environ, 95, 164-176, doi:10.1016/J.Rse.2004.12.011, 2005.

1366 | Zhao, M. S., and Running, S. W.: Drought-Induced Reduction in Global Terrestrial Net
1367 | Primary Production from 2000 Through 2009, Science, 329, 940-943,
1368 | doi:10.1126/Science.1192666, 2010.

1369 | Zheng, Y., Unger, N., Barley, M., and Yue, X.: Relationships between photosynthesis
1370 | and formaldehyde as a probe of isoprene emission, Atmos. Chem. Phys., ~~15~~, ~~8559-~~
1371 | ~~8576~~, doi:10.5194/~~acp-15-8559-2015~~, 2015.

1372 | Zhu, Z. C., Bi, J., Pan, Y. Z., Ganguly, S., Anav, A., Xu, L., Samanta, A., Piao, S. L.,
1373 | Nemani, R. R., and Myneni, R. B.: Global Data Sets of Vegetation Leaf Area Index
1374 | (LAI)3g and Fraction of Photosynthetically Active Radiation (FPAR)3g Derived
1375 | from Global Inventory Modeling and Mapping Studies (GIMMS) Normalized
1376 | Difference Vegetation Index (NDVI3g) for the Period 1981 to 2011, Remote Sens, 5,
1377 | 927-948, doi:10.3390/Rs5020927, 2013.

1378
1379

Xu Yue 10/6/15 1:41 PM
Deleted: Model

Xu Yue 10/6/15 1:41 PM
Deleted: in press

Xu Yue 10/6/15 1:41 PM
Deleted: Discuss.,

Xu Yue 10/6/15 1:41 PM
Deleted: 6037-6080

Xu Yue 10/6/15 1:41 PM
Deleted: bgd

Xu Yue 10/6/15 1:41 PM
Deleted: 6037

Xu Yue 10/6/15 1:41 PM
Deleted: Discuss.,

Xu Yue 10/6/15 1:41 PM
Deleted: 11763-11797

Xu Yue 10/6/15 1:41 PM
Deleted: acpd

Xu Yue 10/6/15 1:41 PM
Deleted: 11763

1390
1391
1392
1393

Table 1. Summary of model simulations driven with WFDEI reanalysis.

Simulations	Descriptions
CO2_MET_LUC	Annually updated [CO ₂] and land cover, and hourly meteorology. All forcings vary for 1980-2011.
CO2_MET	Annually updated [CO ₂] and hourly meteorology for 1980-2011, land cover is prescribed at the year 1980.
CO2_ONLY	Annually updated [CO ₂] for 1980-2011, land cover is prescribed and hourly meteorology is recycled for the year 1980.
MET_ONLY	Hourly meteorology varies for 1980-2011. [CO ₂] and land cover are prescribed at the year 1980.
LUC_ONLY	Annually updated land cover for 1980-2011, [CO ₂] is prescribed and hourly meteorology is recycled for the year 1980.
TEMP_ONLY	Hourly temperature for 1980-2011 but other meteorological variables are recycled for 1980. [CO ₂] and land cover are prescribed at the year 1980.
PAR_ONLY	Hourly PAR for 1980-2011 but other meteorological variables are recycled for 1980. [CO ₂] and land cover are prescribed at the year 1980.
SOILW_ONLY	Hourly soil wetness for 1980-2011 but other meteorological variables are recycled for 1980. [CO ₂] and land cover are prescribed at the year 1980.
LAI_ONLY	Hourly meteorology is recycled for the year 1980. [CO ₂] and land cover are prescribed at the year 1980. Leaf area index varies for 1980-2011.
PHEN_ONLY	Hourly meteorology is recycled for the year 1980. [CO ₂] and land cover are prescribed at the year 1980. Phenology varies for 1980-2011.

1394
1395
1396
1397
1398
1399

1400
 1401
 1402
 1403
 1404
 1405
 1406

Table 2. Summary of trends in different domains from the simulation CO2_MET_LUC, which is driven with WFDEI meteorology. Significant trends ($p < 0.05$) are indicated with asterisks.

Regions	Amazon	North America	Central Africa	Europe	East Asia	Indonesia
LAI ($10^{-3} \text{ m}^2 \text{ m}^{-2} \text{ a}^{-1}$)	0.8	0.4 _*	1.8 _*	3.5 _*	-0.4 _*	-0.1
GPP (Tg C a^{-2})	52.7 _*	13.6	83.3 _*	53.4 _*	42.4 _*	15.3 _*
NPP (Tg C a^{-2})	27.1 _*	9.7	51.7 _*	33.2 _*	27.2 _*	11.4 _*
NEP (Tg C a^{-2})	-8.1	-1.7	11.6	6.7	-6.2	0.2
Ra (Tg C a^{-2})	25.6 _*	3.9	31.6 _*	20.2 _*	15.2 _*	3.9 _*
Rh (Tg C a^{-2})	35.2 _*	11.2 _*	39.8 _*	26.6 _*	33.4 _*	11.2 _*
Isoprene PS_BVOC (Tg C a^{-2})	0.04	-0.03	0.25 _*	0.16 _*	-0.02	-0.01
Isoprene MEGAN (Tg C a^{-2})	-0.43 _*	-0.07 _*	-0.14 _*	0.10 _*	-0.13 _*	-0.16 _*
Monoterpene (Tg C a^{-2})	-0.03 _*	0.01	-0.002	0.03 _*	-0.02 _*	-0.02 _*
Budburst (days a^{-1})	N/A ^a	-0.01	N/A	-0.16 _*	-0.15 _*	N/A
Dormancy onset (days a^{-1})	N/A	0.09 _*	N/A	0.16 _*	0.03	N/A
Season extension (days a^{-1})	N/A	0.1 _*	N/A	0.32 _*	0.18 _*	N/A

1407
 1408
 1409

^a Phenology is set to constant for tropical rainforest in the model.

1410
 1411
 1412
 1413
 1414
 1415
 1416

Table 3. Summary of simulated trends of global carbon fluxes (Tg C a⁻²) from different experiments. Simulations are using WFDEI meteorology. Significant trends ($p < 0.05$) are indicated with asterisks.

Simulations	GPP	NPP	NEP	Ra	Rh
CO2_MET_LUC	297.4 ₋ *	185.3 ₋ *	2.7	112.1 ₋ *	180.9 ₋ *
CO2_MET	329.5 ₋ *	206.2 ₋ *	4.5	123.3 ₋ *	199.8 ₋ *
CO2_ONLY	412.4 ₋ *	299 ₋ *	66.2 ₋ *	113.5 ₋ *	231.9 ₋ *
MET_ONLY	-108.6 ₋ *	-108.2 ₋ *	-72.6 ₋ *	-0.4	-35
LUC_ONLY	-13 ₋ *	-8 ₋ *	-34.6 ₋ *	-5 ₋ *	26.9 ₋ *
TEMP_ONLY	-23.2 ₋ *	-56 ₋ *	-10.2 ₋ *	32.8 ₋ *	-43.6 ₋ *
PAR_ONLY	-5.9	-5.8	-23.4 ₋ *	-0.1	18.3 ₋ *
SOILW_ONLY	-84.8 ₋ *	-51 ₋ *	-13.1 ₋ *	-33.8 ₋ *	-38.3
LAI_ONLY	-8.8	-25.6 ₋ *	-44.5 ₋ *	16.7 ₋ *	18.7 ₋ *
PHEN_ONLY	-103.1 ₋ *	-56.2 ₋ *	47.1 ₋ *	-46.8 ₋ *	-102.9 ₋ *

1417
 1418

Xu Yue 10/6/15 1:41 PM
Deleted: Results based on MERRA meteorology are shown in Table S1

1421 **Figure Captions**

1422

1423 **Figure 1.** Comparison of trends in (b-f) simulated leaf area index (LAI) with (a)
1424 observations for 1982-2011. Observations are derived from GIMMS NDVI. Simulations
1425 are performed with either (d, e, f) single forcings or (b, c) the combinations of these
1426 forcings. Forcings considered include meteorology from WFDEI reanalysis (MET), CO₂
1427 fertilization (CO2), and land use change (LUC). For every forcing included in the
1428 simulation, the year-to-year fields are utilized. Otherwise, the forcing is prescribed at the
1429 year 1980. Only significant trends ($p < 0.05$) are presented. The six box regions in (a)
1430 indicate areas for statistical analyses in Table 2.

1431

1432 **Figure 2.** Simulated trends in (a) gross primary productivity (GPP), (c) net primary
1433 productivity (NPP), and (e) net ecosystem productivity (NEP), and (b, d, f) the dominant
1434 drivers for these changes during 1982-2011. Simulations are performed with WFDEI
1435 reanalysis. Three factors, meteorological forcing, CO₂ fertilization, and land use change,
1436 are considered as the potential drivers of flux trends. For each grid, in figures (b, d, f), the
1437 factor generating the largest (either maximum or minimum) trend with the same sign as
1438 the net change (a, c, e) is selected as the driving factor. Only significant trends ($p < 0.05$)
1439 are presented.

1440

1441 **Figure 3.** Comparisons of trends in (a, b) GPP and (c, d) NPP for 2000-2011 between (a,
1442 c) simulations and (b, d) observations. Observed fluxes are retrieved from the Moderate
1443 Resolution Imaging Spectroradiometer (MODIS).

1444

1445 **Figure 4.** Simulated (a) trends in GPP driven alone with WFDEI reanalysis, and the (b)
1446 drivers for such changes. Simulation in (a) is performed with year-to-year meteorological
1447 forcings but prescribed [CO₂] and land use in the year 1980. Simulations in (b) are the
1448 same as (a), except that the year-to-year variations are allowed only for a single
1449 meteorological variable (temperature, PAR, or soil wetness) each time. For each grid, the
1450 meteorological variable generating the largest (either maximum or minimum) trend with

- Xu Yue 10/6/15 1:41 PM
Deleted: b
- Xu Yue 10/6/15 1:41 PM
Deleted: c
- Xu Yue 10/6/15 1:41 PM
Deleted: -
- Xu Yue 10/6/15 1:41 PM
Deleted: ,
- Xu Yue 10/6/15 1:41 PM
Deleted: -
- Xu Yue 10/6/15 1:41 PM
Deleted: Results for simulations with MERRA reanalysis are shown in Fig. S1.
- Xu Yue 10/6/15 1:41 PM
Deleted: (a)
- Xu Yue 10/6/15 1:41 PM
Deleted: and (b) MERRA
- Xu Yue 10/6/15 1:41 PM
Deleted: ,
- Xu Yue 10/6/15 1:41 PM
Deleted: c-d
- Xu Yue 10/6/15 1:41 PM
Deleted: Simulations
- Xu Yue 10/6/15 1:41 PM
Deleted: and (b) are
- Xu Yue 10/6/15 1:41 PM
Deleted: c) and (d)
- Xu Yue 10/6/15 1:41 PM
Deleted: and (b) respectively,

1466 | the same sign as the net change (a) is selected as the driving factor. Only significant
1467 | trends ($p < 0.05$) are presented.

1468

1469 | **Figure 5.** Global total fluxes of GPP, NPP, Rh (heterotrophic respiration), and NEP from
1470 | different sensitivity simulations with all forcings (black), meteorology alone (red), CO₂
1471 | alone (green), and land use change alone (blue).

1472

1473 | **Figure 6.** Simulated trends of (a, c) isoprene and (e) monoterpene, and (b, d, f) the
1474 | dominant drivers for these changes during 1982-2011. Simulations are performed with
1475 | WFDEI reanalysis. Isoprene emissions are simulated with (a) PS_BVOC and (c)
1476 | MEGAN schemes. Three factors, meteorological forcing, CO₂ effects (both fertilization
1477 | and inhibition), and land use change, are considered as the potential drivers of flux
1478 | trends. For each grid, in figures (b, d, f), the factor generating the largest (either maximum
1479 | or minimum) trend with the same sign as the net change (a-c) is selected as the driving
1480 | factor. Only significant trends ($p < 0.05$) are presented.

1481

1482 | **Figure 7.** Responses of (a) GPP and (b) isoprene emissions to the changes in the annual
1483 | average LAI at the north of 30°N for simulations CO₂_MET (red) and LAI_ONLY
1484 | (blue). Both GPP and isoprene emissions are the sum of all PFTs. Isoprene is simulated
1485 | with the PS_BVOC scheme. Units of trends are (a) Pg C a⁻¹ LAI⁻¹ and (b) Tg C a⁻¹ LAI⁻¹.
1486 | The spatial distribution of GPP and isoprene changes is shown in Figure S2.

1487

1488 | **Figure 8.** Predicted trend in (a) budburst and (b) dormancy onset dates over north of
1489 | 30°N and the responses of (c) GPP and (d) isoprene emissions to the changes in the
1490 | growing length. Both GPP and isoprene emissions are the sum of DBF, shrub, grassland,
1491 | and tundra. Isoprene is simulated with the PS_BVOC scheme. For the bottom panel,
1492 | different colors indicate sensitivity experiments with different year-to-year forcings: CO₂
1493 | and meteorology (red), temperature only (magenta), and phenology only (blue). Units of
1494 | trends are (a) day a⁻¹, (b) day a⁻¹, (c) Pg C a⁻¹ day⁻¹, and (d) Tg C a⁻¹ day⁻¹. The spatial
1495 | distribution of GPP and isoprene changes is shown in Figure S2.

1496

Xu Yue 10/6/15 1:41 PM

Deleted: -b

Xu Yue 10/6/15 1:41 PM

Deleted: b

Xu Yue 10/6/15 1:41 PM

Deleted: c

Xu Yue 10/6/15 1:41 PM

Deleted: -

Xu Yue 10/6/15 1:41 PM

Deleted: b

Xu Yue 10/6/15 1:41 PM

Deleted: ,

Xu Yue 10/6/15 1:41 PM

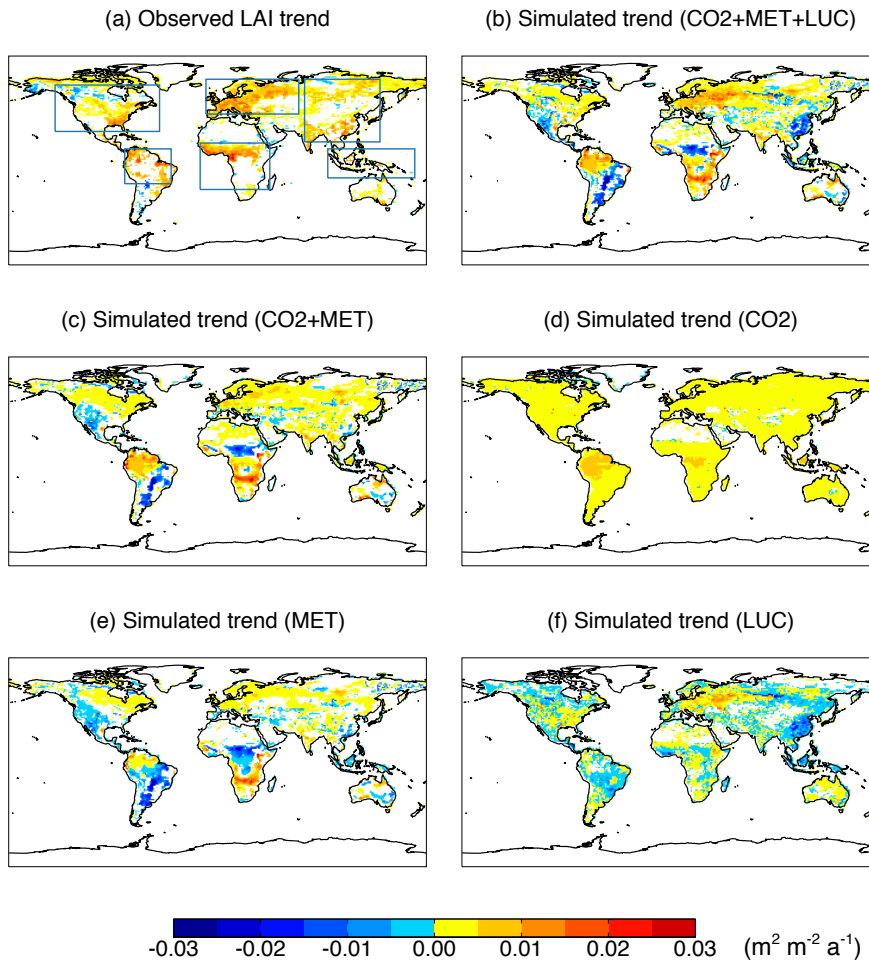
Deleted: Results for simulations with MERRA reanalysis are shown in Fig. S4.

Xu Yue 10/6/15 1:41 PM

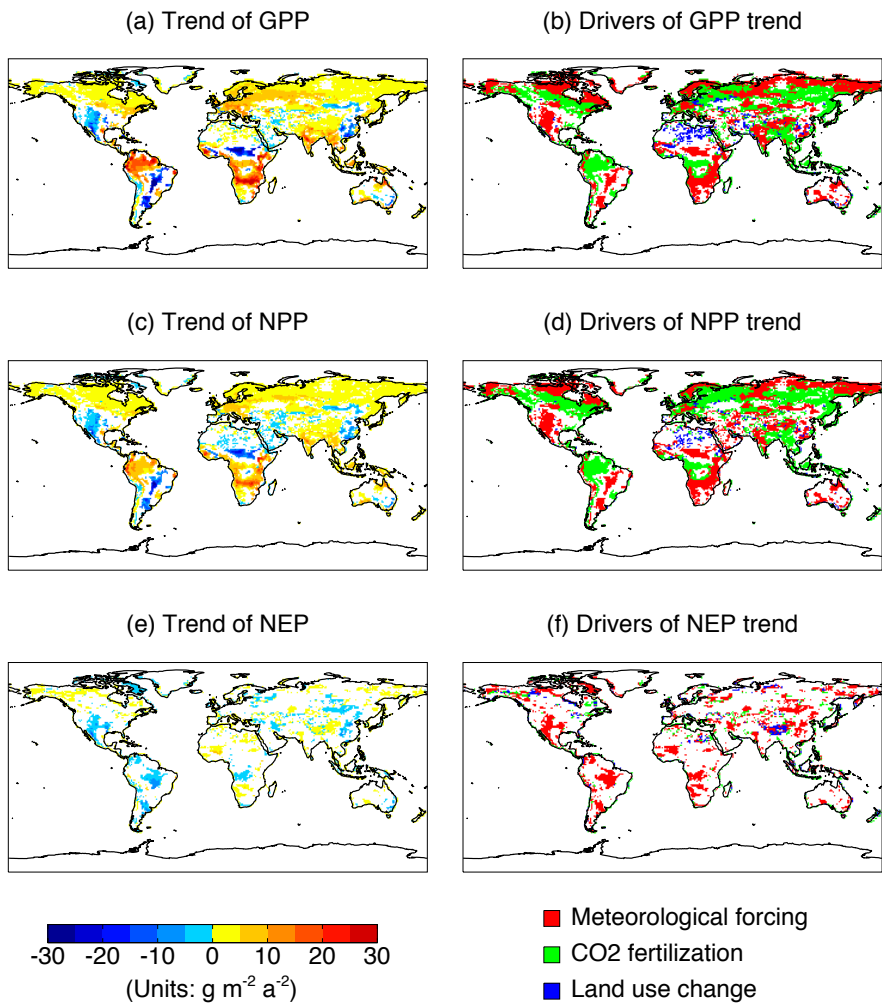
Deleted: S5

Xu Yue 10/6/15 1:41 PM

Deleted: S5



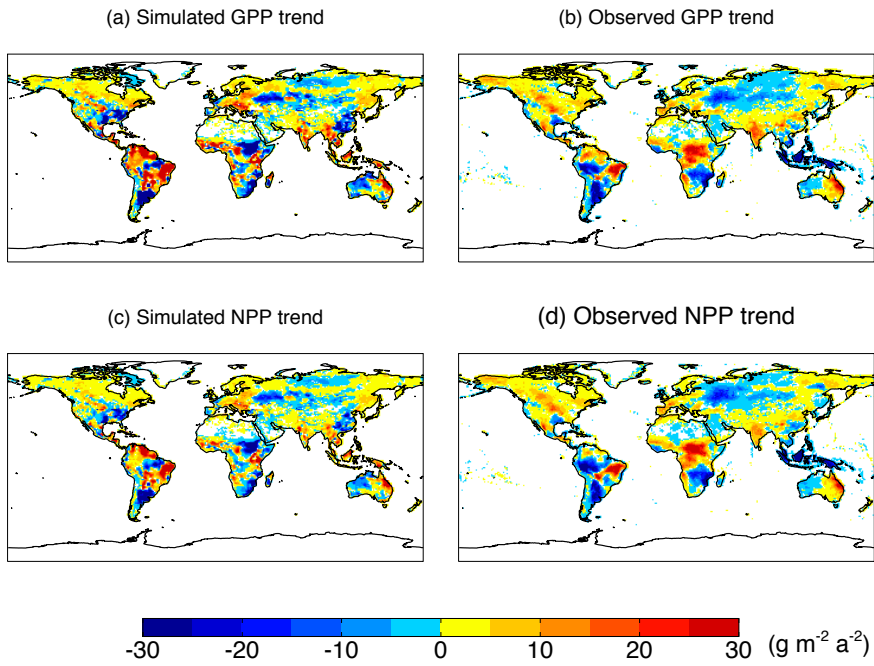
1507
 1508 **Figure 1.** Comparison of trends in (b-f) simulated leaf area index (LAI) with (a)
 1509 observations for 1982-2011. Observations are derived from GIMMS NDVI. Simulations
 1510 are performed with either (d, e, f) single forcings or (b, c) the combinations of these
 1511 forcings. Forcings considered include meteorology from WFDEI reanalysis (MET), CO₂
 1512 fertilization (CO₂), and land use change (LUC). For every forcing included in the
 1513 simulation, the year-to-year fields are utilized. Otherwise, the forcing is prescribed at the
 1514 year 1980. Only significant trends ($p < 0.05$) are presented. The six box regions in (a)
 1515 indicate areas for statistical analyses in Table 2.
 1516
 1517
 1518



1519
1520
1521
1522
1523
1524
1525
1526
1527
1528
1529

Figure 2. Simulated trends in (a) gross primary productivity (GPP), (c) net primary productivity (NPP), and (e) net ecosystem productivity (NEP), and (b, d, f) the dominant drivers for these changes during 1982-2011. Simulations are performed with WFDEI reanalysis. Three factors, meteorological forcing, CO₂ fertilization, and land use change, are considered as the potential drivers of flux trends. For each grid in figures (b, d, f), the factor generating the largest (either maximum or minimum) trend with the same sign as the net change (a, c, e) is selected as the driving factor. Only significant trends ($p < 0.05$) are presented.

1530
1531



1532
1533 **Figure 3.** Comparisons of trends in (a, b) GPP and (c, d) NPP for 2000-2011 between (a,
1534 c) simulations and (b, d) observations. Observed fluxes are retrieved from the Moderate
1535 Resolution Imaging Spectroradiometer (MODIS).

1536
1537
1538
1539
1540
1541
1542

1543
1544
1545
1546
1547
1548
1549
1550
1551
1552
1553
1554
1555
1556
1557
1558
1559
1560
1561
1562
1563
1564
1565
1566
1567
1568
1569
1570
1571
1572
1573
1574
1575
1576
1577
1578
1579
1580
1581

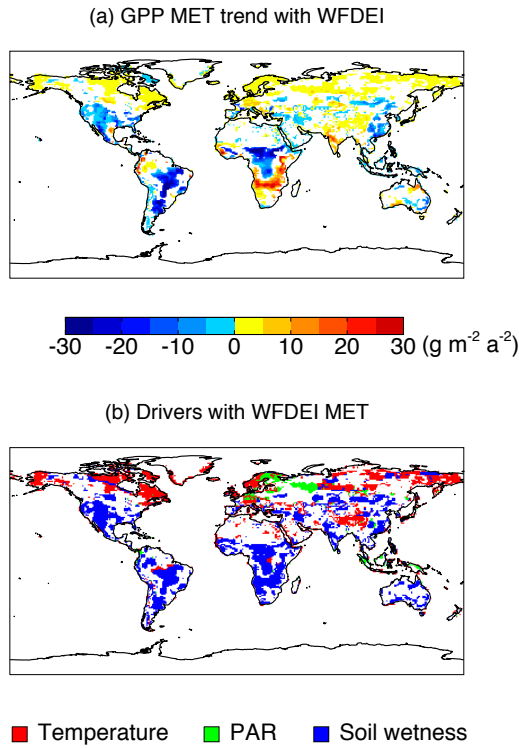
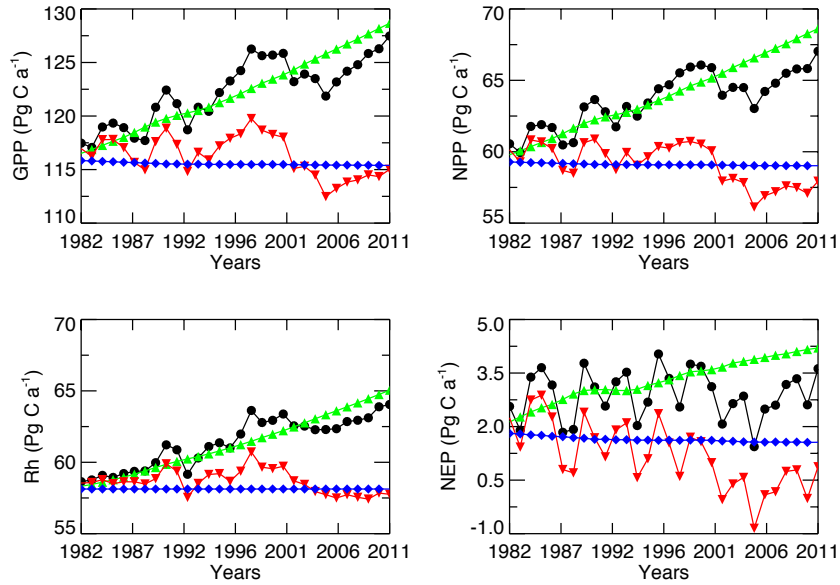
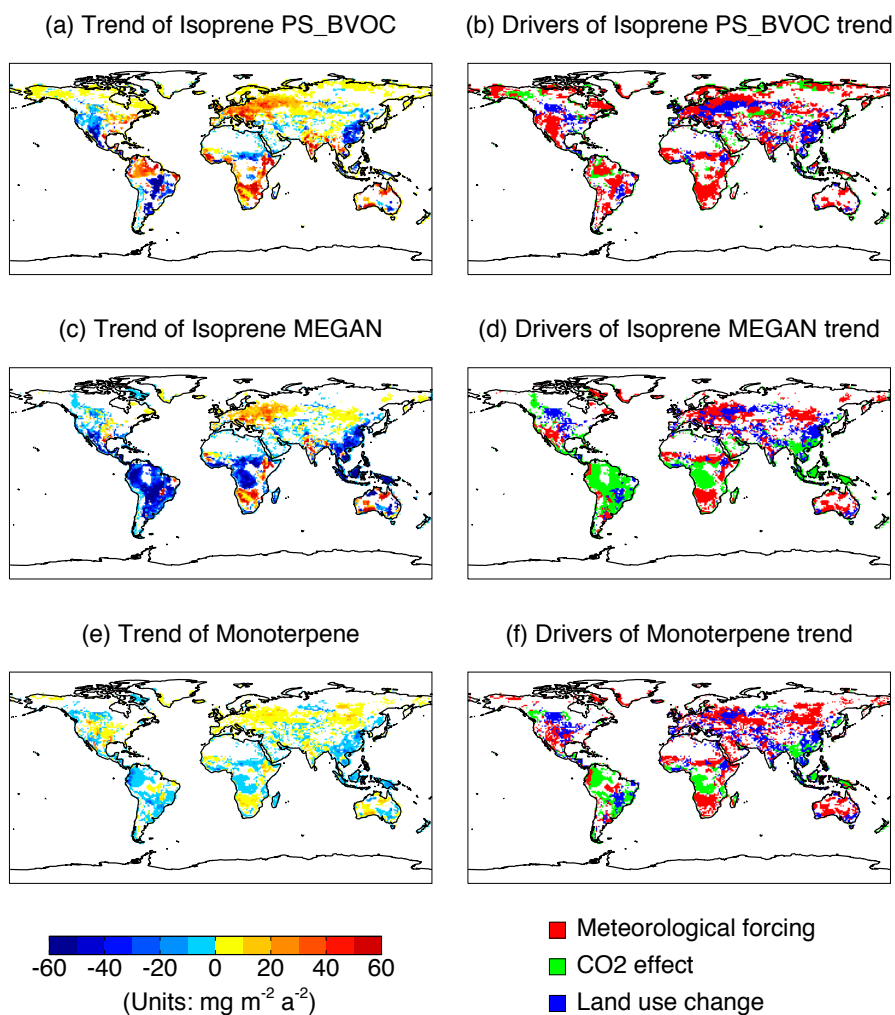


Figure 4. Simulated (a) trends in GPP driven alone with WFDEI reanalysis and the (b) drivers for such changes. Simulation in (a) is performed with year-to-year meteorological forcings but prescribed $[\text{CO}_2]$ and land use in the year 1980. Simulations in (b) are the same as (a) except that the year-to-year variations are allowed only for a single meteorological variable (temperature, PAR, or soil wetness) each time. For each grid, the meteorological variable generating the largest (either maximum or minimum) trend with the same sign as the net change (a) is selected as the driving factor. Only significant trends ($p < 0.05$) are presented.

1582
1583
1584
1585
1586
1587



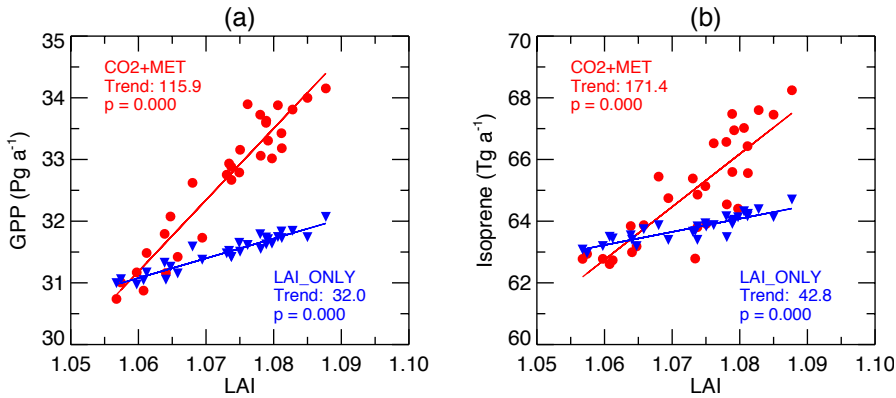
1588 **Figure 5.** Global total fluxes of GPP, NPP, Rh (heterotrophic respiration), and NEP from
1589 different sensitivity simulations with all forcings (black), meteorology only (red), CO₂
1590 alone (green), and land use change alone (blue).
1591



1592
1593
1594
1595
1596
1597
1598
1599
1600
1601

Figure 6. Simulated trends of (a, c) isoprene and (e) monoterpene, and (b, d, f) the dominant drivers for these changes during 1982-2011. Simulations are performed with WFDEI reanalysis. Isoprene emissions are simulated with (a) PS_BVOC and (c) MEGAN schemes. Three factors, meteorological forcing, CO₂ effects (both fertilization and inhibition), and land use change, are considered as the potential drivers of flux trends. For each grid in figures (b, d, f), the factor generating the largest (either maximum or minimum) trend with the same sign as the net change (a-c) is selected as the driving factor. Only significant trends ($p < 0.05$) are presented.

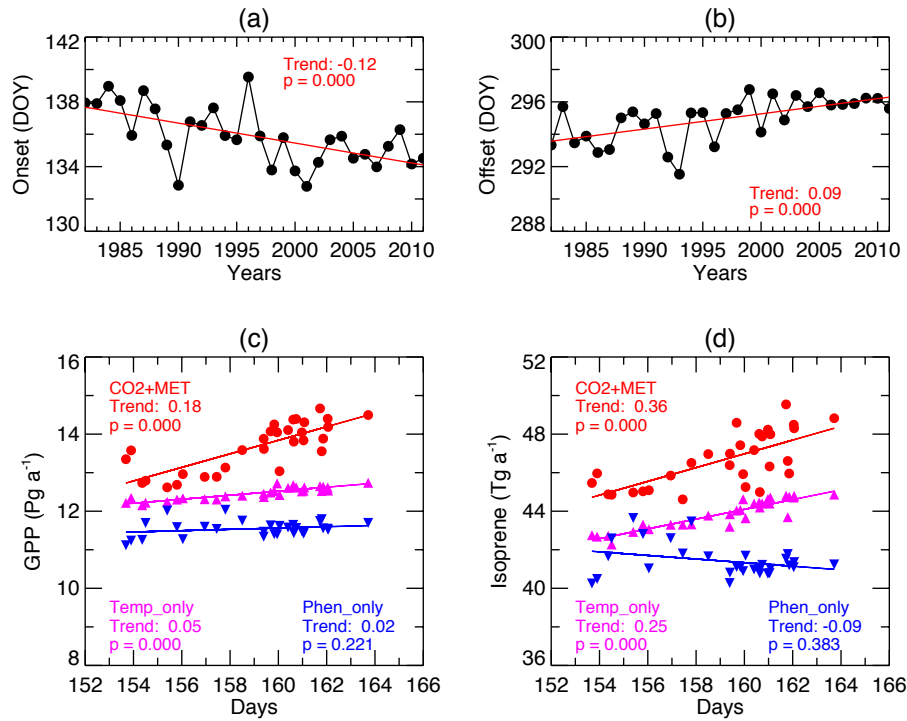
1602
1603
1604
1605
1606



1607
1608
1609
1610
1611
1612
1613
1614

Figure 7. Responses of (a) GPP and (b) isoprene emissions to the changes in the annual average LAI at the north of 30°N for simulations CO2_MET (red) and LAI_ONLY (blue). Both GPP and isoprene emissions are the sum of all PFTs. Isoprene is simulated with the PS_BVOC scheme. Units of trends are (a) Pg C a⁻¹ LAI⁻¹ and (b) Tg C a⁻¹ LAI⁻¹. The spatial distribution of GPP and isoprene changes is shown in Figure S2.

1615
1616



1617

1618 **Figure 8.** Predicted trend in (a) budburst and (b) dormancy onset dates over north of
1619 30°N and the responses of (c) GPP and (d) isoprene emissions to the changes in the
1620 growing length. Both GPP and isoprene emissions are the sum of DBF, shrub, grassland,
1621 and tundra. Isoprene is simulated with the PS_BVOC scheme. For the bottom panel,
1622 different colors indicate sensitivity experiments with different year-to-year forcings: CO₂
1623 and meteorology (red), temperature only (magenta), and phenology only (blue). Units of
1624 trends are (a) day a⁻¹, (b) day a⁻¹, (c) Pg C a⁻¹ day⁻¹, and (d) Tg C a⁻¹ day⁻¹. The spatial
1625 distribution of GPP and isoprene changes is shown in Figure S2.

1626

1627

1628